Influence of Thermal Aging on the Microstructure and Mechanical Behavior of Dual Phase Precipitation Hardened Powder Metallurgy Stainless Steels

by

Jennifer Stewart

A Thesis Presented in Partial Fulfillment
of the Requirements for the Degree
Master of Science

Approved April 2011 by the
Graduate Supervisory Committee:

Nikhilesh Chawla, Chair
Hanqing Jiang
Stephen Krause

ARIZONA STATE UNIVERSITY

May 2011

ABSTRACT

Increasing demand for high strength powder metallurgy (PM) steels has resulted in the development of dual phase PM steels. In this work, the effects of thermal aging on the microstructure and mechanical behavior of dual phase precipitation hardened powder metallurgy (PM) stainless steels of varying ferrite-martensite content were examined. Quantitative analyses of the inherent porosity and phase fractions were conducted on the steels and no significant differences were noted with respect to aging temperature. Tensile strength, yield strength, and elongation to fracture all increased with increasing aging temperature reaching maxima at 538^{o}C in most cases. Increased strength and decreased ductility were observed in steels of higher martensite content. Nanoindentation of the individual microconstituents was employed to obtain a fundamental understanding of the strengthening contributions. Both the ferrite and martensite hardness values increased with aging temperature and exhibited similar maxima to the bulk tensile properties.

Due to the complex non-uniform stresses and strains associated with conventional nanoindentation, micropillar compression has become an attractive method to probe local mechanical behavior while limiting strain gradients and contributions from surrounding features. In this study, micropillars of ferrite and martensite were fabricated by focused ion beam (FIB) milling of dual phase precipitation hardened powder metallurgy (PM) stainless steels. Compression testing was conducted using a nanoindenter equipped with a flat punch indenter. The stress-strain curves of the individual microconstituents were calculated from

the load-displacement curves less the extraneous displacements of the system. Using a rule of mixtures approach in conjunction with porosity corrections, the mechanical properties of ferrite and martensite were combined for comparison to tensile tests of the bulk material, and reasonable agreement was found for the ultimate tensile strength. Micropillar compression experiments of both as sintered and thermally aged material allowed for investigation of the effect of thermal aging.

DEDICATION

This thesis is dedicated to my husband, Joe, and my parents, Linda and Frank Boydston, for their patience and support without which this project would not have been possible.

ACKNOWLEDGMENTS

I would sincerely like to thank my graduate advisor, Dr. Nikhilesh Chawla, for his endless mentorship, guidance, and patience and for providing me access to his lab and staff. In addition, I would like to recognize Dr. Jason Williams for also being a great mentor and for his help with tensile testing, scanning electron microscopy, and general lab technique and Dr. Ling Jiang and Dr. Danny Singh for their assistance with nanoindentation and FIB milling over many late nights. Special thanks are also given to Hoeganaes Corporation for providing the materials and financial support for this research and Dr. Chris Schade and Dr. Thomas Murphy for stimulating discussions related to this work. I would also like to thank my additional committee members, Dr. Hanqing Jiang and Dr. Stephen Krause, for your commitment to my end goal. Lastly, I would like to recognize my employer, Intel Corporation, and managers, Jacqueline Wood and Sharen Rembelski, for their support and special accommodations without which this work would not be possible.

TABLE OF CONTENTS

Page

CHAPTER Page

LIST OF TABLES

Table Page

LIST OF FIGURES

Figure Page

Figure Page

Chapter 1

INTRODUCTION

PM is used extensively in the automotive sector due to its low cost as a production technique, its capability of manufacturing complex shapes, and its long term performance reliability. However, many of these applications require high strength and wear resistant materials which has resulted in the development of dual phase PM stainless steels. Dual phase steels generally offer a good balance of high strength and reasonable ductility resulting from their unique microstructure in which martensite provides strength while ferrite imparts ductility. Intuitively, by adjusting the phase fractions of these microconstituents, the mechanical properties of the resulting composite microstructure may be tuned. Furthermore, optional finishing steps such as thermal aging may also be used to adjust the mechanical properties of dual phase steels. Dual phase steels often contain a complex mix of alloying elements, primarily including ferrite and austenite stabilizers to achieve the dual phase structure, but may also include elements known to induce precipitation hardening such as aluminum and copper. The presence of these precipitation hardening elements may enhance the dual phase steel's response to thermal aging.

In this study, the microstructure and mechanical behavior of dual phase precipitation hardened PM stainless steels of varying ferrite and martensite content are examined. Both the composite steel behavior and contributions from the individual microconstituents are evaluated by several techniques including tensile testing, nanoindentation, and micropillar fabrication and compression.

Furthermore, the effect of aging temperature is examined. Following a brief review of the available literature Chapter 2, the microstructure and mechanical behavior of two sets of dual phase steels, designated low martensite (LM) and high martensite (HM) due to their varying phase fractions, are examined in Chapter 3. Conventional sharp tip nanoindentation of the individual microconstituents is used to explain the composite steel properties of the bulk steels. However, due to the complex strain gradients present in conventional nanoindentation, a more quantitative approach involving micropillar fabrication and compression of the individual microconstituents is used in Chapter 4 to determine the strength of ferrite and martensite in an attempt to model the bulk steels' mechanical properties.

Chapter 2

REVIEW OF LITERATURE

2.1 Powder Metallurgy

PM is a metallurgical production technique involving the compaction of atomized metal powders, which are often treated with organic binders to promote adhesion, into a net shape followed by sintering to complete solidification. This technique offers a wide variety of advantages over its wrought counterparts including applicability to a wide variety of alloy systems, production of complex shapes, part-to-part uniformity, long term performance reliability, minimal scrap loss, and cost effectiveness [1] and therefore finds uses in many applications. However, as a result of the production technique, PM materials contain inherent porosity which strongly influences the mechanical behavior. The presence of pores leads to early onset of plasticity and localization of strain due to reduction of the load bearing cross-sectional area [2], the stress concentration effect of angular pores [3], the potential for microcrack initiation at pores [4-6] and the inherent inhomogeneity of pore distribution [6-8]. Hence, fracture in PM materials is primarily controlled by porosity.

The size, shape, and distribution of pores are also known to affect fracture. Chawla and Deng [9] examined sintered steel and found that as the fraction of porosity increased, the size and irregularity of pores also increased. Irregular pore shape introduces a notch effect and causes high stress concentration at pores resulting in localized slip leading to crack initiation [4, 10]. Nonhomogeneous pore distribution may also affect mechanical behavior because plasticity may

initiate at pore clusters due to higher localized stress intensity [6-8]. Fracture occurs by crack propagation or void coalescence between closely neighboring pores. This is the preferred route due to decreased matrix ligament size in areas of pore clustering.

Several authors have developed relationships to relate strength to porosity [11-18] but with limited universal success due to complex nature of porosity (shape, size, morphology, and distribution) and its effects on microstructure. Furthermore, relationships developed from empirical data may at best only estimate a range of strengths for a given porosity. A review of some of these relationships is presented in Chapter 4 for review.

2.2 Dual Phase Steels

The increasing demand for high strength PM steels has led to the development of dual phase stainless steels [19]. The dual phase steel microstructure consists of both martensite and ferrite microconstituents and is achieved through the use of austenite and ferrite stabilizers in the alloy coupled with specific processing conditions. In addition, low carbon concentration in the alloy is necessary to coincide with the two phase austenite-ferrite region of the Fe-C phase diagram. At higher temperatures, the steel is composed of ferrite and austenite but upon cooling, the austenite converts to martensite and the dual phase ferrite-martensite microstructure is achieved. This transformation is known to cause high dislocation density in ferrite near martensite-ferrite interfaces [20-21] and high residual stresses [21-23], both of which affect the steel's mechanical behavior.

Because of the complex microstructures and mechanisms involved, dual phase steels are known to exhibit continuous yielding behavior (i.e. no defined yield point), high work hardening rate, low yield strength, and high ultimate tensile strength [24]. Dual phase steels also benefit from their composite microstructure in that that martensite imparts strength while ferrite imparts ductility. Furthermore, the high strength of these steels results from grain boundary strengthening, through impedance of dislocation motion by grain boundaries, and is increased by the presence of grain boundaries between similar and dissimilar phases [19]. The mechanical properties of dual phase steels and their microconstituents are also dependent on alloy and phase chemistry, thermal processing, phase fraction and size, internal stresses, and precipitate content to name a few [24].

Intuitively, by adjusting the phase fractions of martensite and ferrite, the mechanical properties of dual phase steels may be tuned. As such, many studies have been conducted to determine the effect of phase fraction on mechanical properties. Many authors have found that strength increases linearly with increasing martensite volume fraction in accordance with the rule of mixtures [23, 25-30]. By conventional composite strengthening, as the fraction of the harder phase, in this case martensite, is increased, the strength of the composite is increased. Somewhat contradictory results have been obtained in which the strength of the composite increased linearly up to a martensite volume fraction of approximately 55%, after which the strength gradually decreased [31]. This behavior was attributed to a decrease in strength of the martensite due to lower

local carbon concentration in martensite at higher martensite volume fraction. The decreased carbon content allows for easier dislocation motion and hence lower strength. However, most literature sources on this topic suggest that an entirely linear relationship exists between strength and martensite fraction. In addition, several rule of mixtures relationships have been developed to describe the mechanical behavior of the composite microstructure based on the phase fractions and mechanical properties of the microconstituents [25-26, 32]. Refinements in the microstructure, such as grain size and shape [23, 27-29, 33] and martensite continuity [34] have also been shown to influence the strength of the steel, and thus phase fraction is not the sole microstructural determinant for mechanical behavior.

2.3 Thermal Aging

The technique of thermal aging is often employed to alter the mechanical properties of ferritic and/or martensitic steels and is also applicable to PM. In traditional martensite-containing steels, strength generally decreases while ductility increases with increasing thermal exposure due to tempering of the martensite. During this process, carbon diffuses out of the martensite and the tetragonal distortion of the phase is reduced, resulting in decreased residual stresses and strength of the steel composite. However, by introducing precipitation hardening elements such as copper or aluminum, dual phase steels may be, instead, strengthened through thermal exposure [19, 35-39]. First, the steel is heated to a high temperature such that diffusion of the alloying elements occurs and a supersaturated solution is formed. Second, the steel is quenched and

then heated to intermediate temperatures at which the supersaturated solution decomposes and precipitates are formed which may impede dislocation motion through Orowan bowing [40] and strengthen the material. A balance of strength and ductility may thus be achieved through precipitation hardening and tempering of martensite, respectively.

2.4 Nanoindentation

Conventional nanoindentation is an attractive technique to investigate the properties of the individual martensite and ferrite microconstituents in dual phase steels. Small indentation sizes allow for individual phases to be probed while avoiding effects from surrounding features. Previous studies have utilized nanoindentation in various steels to examine the effects of grain size [41-44], grain boundary strengthening [43, 45-47], indentation size dependent strengthening [41], carbon concentration [38, 47-48] thermal aging [38, 45, 48-51], and precipitation hardening [40] on the mechanical properties of ferritic and/or martensitic steels. To date, very few nanoindentation studies [41, 50-51] have been conducted on dual phase steels and to my knowledge none have related these data to bulk tensile test results. Furthermore, the effect of precipitation hardening from copper in dual phase steels has previously not been explored with nanoindentation.

Separation of contributions from the individual microconstituents to the mechanical behavior of composite dual phase steels has proven difficult due to mechanisms present at the micron scale. Conventional nanoindentation using a sharp tip Berkovich indenter has been used to probe the local mechanical

properties of dual steels [40, 50-51] but is limited to the determination of the Young's modulus and nanoindentation hardness of the microconstituents. Due to confinement of plastic deformation to a very small volume, non-uniform strain and stress distributions result. So-called indentation size effects are attributed to these strain gradients as addressed by the strain gradient theory [52]. Furthermore, contributions from surrounding features, such as mutual constraint between two phases or grain boundary effects, cannot be removed from conventional nanoindentation experiments.

2.5 Micropillar Compression

Micropillar compression consists of the fabrication of free-standing pillars in the low micron to nanometer scale, which can be isolated to individual phases, followed by compression using a nanoindenter equipped with a flat punch. It is an attractive complementary technique to nanoindentation because the non-uniform stress and strain distributions associated with sharp tip indentation may be removed and the strength of individual microconstituents may be determined. Most research in this area has focused on the behavior of single crystals such as gold [53-55] and nickel and its alloys [56-58] and again size effects were noted in which increased strength accompanies decreased pillar size [53-61]. This phenomenon has been explained both by dislocation starvation/exhaustion [53-56, 58-60] and dislocation pile-up [59]. In the former, small pillar sizes result in low dislocation density which is quickly exhausted during deformation due to dislocation annihilation at the pillar's surface. This leads to dislocation starved conditions in which increased stress is needed to nucleate dislocations to

accommodate deformation and hence increased strength results. In dislocation pile-up, dislocations group in the pillar interior resulting in high pile-up stresses which shield dislocation sources, leading to increased flow stress and therefore strength.

Pouchon et al. performed micropillar compression studies of irradiated oxide dispersion strengthened (ODS) ferritic steel alloys and compared micropillar compression results to those of tensile tests [62]. Conversely to the case of relatively defect-free single crystals as described above, size effects were not noted for this material. This conclusion was drawn from reasonable matching between tensile tests and micropillar compression data and is attributed to the inherent defect density of the ODS ferritic steel. This suggests that application of micropillar compression testing to the dual phase steels in the current study is a reasonable approach and that the results should not suffer from size effects since the current dual phase steels contain defects such as dislocations, precipitates, etc. To my knowledge, Pouchon's work is the only available steel micropillar compression study available in the literature.

Chapter 3

MICROSTRUCTURAL ANALYSIS, TENSILE TESTING, AND MICROCONSTITUENT CHARACTERIZATION BY CONVENTIONAL NANOINDENTATION

3.1 Abstract

The effects of thermal aging on the microstructure and mechanical behavior of dual phase precipitation hardened powder metallurgy (PM) stainless steels of varying ferrite-martensite content were examined. Quantitative analyses of the inherent porosity and phase fractions were conducted on the steels and no significant differences were noted with respect to aging temperature. Tensile strength, yield strength, and elongation to fracture all increased with increasing aging temperature reaching maxima at 538^{o}C in most cases. Increased strength and decreased ductility were observed in steels of higher martensite content. Nanoindentation of the individual microconstituents was employed to obtain a fundamental understanding of the strengthening contributions. Both the ferrite and martensite nanohardness values increased with aging temperature and exhibited similar maxima to the bulk tensile properties.

3.2 Introduction

Powder metallurgy (PM) offers many advantages including applicability to a wide variety of alloy systems, production of complex shapes, part-to-part uniformity, long term performance reliability, minimal scrap loss, and cost effectiveness [1]. Similar to wrought counterparts, PM parts can be produced with a wide variety of microstructures to tailor mechanical behavior. They may

also be heat-treated for increased strength and/or wear resistance. Early onset of plasticity and localization of strain takes place in these materials, however, due to reduction of the load bearing cross-sectional area [2], the stress concentration effect of angular pores [3], the potential for microcrack initiation at pores [4-6], and the inherent inhomogeneity of pore distribution [6-8]. All of these factors are detrimental to the mechanical properties of porous steels.

The increasing demand for high strength PM steels has led to the development of dual phase stainless steels [9]. The dual phase steel microstructure consists of both martensite and ferrite microconstituents and is achieved through the use of austenite and ferrite stabilizers in the alloy coupled with specific processing conditions. In addition, low carbon concentration in the alloy is necessary to coincide with the two phase austenite-ferrite region of the Fe-C phase diagram. At higher temperatures, the steel is composed of ferrite and austenite but upon cooling, the austenite converts to martensite and the dual phase ferrite-martensite microstructure is achieved. This transformation is known to cause high dislocation density in ferrite near martensite-ferrite interfaces [10-11] and high residual stresses [11-13], both of which affect the steel's mechanical behavior.

Because of the complex microstructures and mechanisms involved, dual phase steels are known to exhibit continuous yielding behavior (i.e. no defined yield point), high work hardening rate, low yield strength, and high ultimate tensile strength [14]. Dual phase steels also benefit from their composite microstructure in that that martensite imparts strength while ferrite imparts

ductility. Furthermore, the high strength of these steels results from grain boundary strengthening, through impedance of dislocation motion by grain boundaries, and is increased by the presence of grain boundaries between similar and dissimilar phases [9]. The mechanical properties of dual phase steels and their microconstituents are also dependent on alloy and phase chemistry, thermal processing, phase fraction and size, internal stresses, and precipitate content to name a few [14].

The mechanical properties of dual phase steels may be tuned by adjusting the volume fractions of the microconstituents. Many authors have studied the effect of increasing the martensite content on the mechanical behavior and have found that strength increases linearly with increasing martensite volume fraction in accordance with the rule of mixtures [13, 15-20]. By conventional composite strengthening, as the fraction of the harder phase, in this case martensite, is increased, the strength of the composite is increased. Somewhat contradictory results have been obtained in which the strength of the composite increased linearly up to a martensite volume fraction of approximately 55%, after which the strength gradually decreased [21]. This behavior was attributed to a decrease in strength of the martensite due to lower local carbon concentration in martensite at higher martensite volume fraction. The decreased carbon content allows for easier dislocation motion and hence lower strength. Refinements in the microstructure, such as grain size and shape [13,17-19, 22] and martensite continuity [23] have also been shown to influence the strength of the steel, and

thus phase fraction is not the sole microstructural determinant for mechanical behavior.

The technique of thermal aging is often employed to alter the mechanical properties of ferritic and/or martensitic steels. In traditional martensite-containing steels, strength generally decreases while ductility increases with increasing thermal exposure due to tempering of the martensite. During this process, carbon diffuses out of the martensite and the tetragonal distortion of the phase is reduced, resulting in decreased residual stresses and strength of the steel composite. However, by introducing precipitation hardening elements such as copper or aluminum, dual phase steels may be, instead, strengthened through thermal exposure [9, 24-28]. First, the steel is heated to a high temperature such that diffusion of the alloying elements occurs and a supersaturated solution is formed. Second, the steel is quenched and then heated to intermediate temperatures at which the supersaturated solution decomposes and precipitates are formed which may impede dislocation motion through Orowan bowing [29] and strengthen the material. A balance of strength and ductility may thus be achieved through precipitation hardening and tempering of martensite, respectively.

One of the challenges in quantifying the composite behavior of dual phase steels is the difficulty, to date, to investigate the properties of the individual martensite and ferrite microconstituents in dual phase steels. In this study, we have used nanoindentation to probe the local mechanical properties of the steels' microconstituents to better understand the composite behavior. This technique is particularly valuable in dual phase steels due to the capability of indenting

individual phases. Previous studies have utilized nanoindentation to examine the effects of grain size [30-33], grain boundary strengthening [32, 34-36], indentation size dependent strengthening [30], carbon concentration [27, 36-37], thermal aging [34, 37-40], and precipitation hardening [29] on the mechanical properties of ferritic and/or martensitic steels. To date, very few nanoindentation studies [30, 39-40] have been conducted on dual phase steels and to our knowledge none have related these data to bulk tensile test results. Furthermore, the effect of precipitation hardening from copper in dual phase steels has previously not been explored with nanoindentation.

In this study, the mechanical behavior and microstructures of dual phase precipitation hardened PM stainless steels, previously developed by Schade et al. [9], of varying martensite/ferrite phase fraction and aging conditions are examined. Nanoindentation of the microconstituents was conducted to gain a deeper understanding of the mechanical properties of the bulk steels and the effects of thermal aging and precipitation hardening on the evolution of mechanical properties.

3.3 Materials and Experimental Procedure

The specimens used in this study were sintered by Hoeganaes Corporation. The nominal composition of the dual phase precipitation hardened (DPPH) steel alloy is shown in Table 1 and includes low carbon concentration (0.013%) and the presence of ferrite stabilizers (chromium, silicon, and molybdenum) and austenite stabilizers (nickel and copper) to achieve the dual phase steel microstructure. The powders were mixed with 0.75 w/o of an organic

binder (Acrawax C, Promaplast, Mexico) and compacted at 386 MPa into standard rectangular with gage and total lengths of approximately 38 mm and 86 mm, respectively. The samples were then sintered for 30 minutes at 1260^{o}C in hydrogen to a density of 6.60 g/cm^{3}. After cooling, the specimens were aged in 100% nitrogen for 1 hour at temperatures ranging from 371^{o}C to 593^{o}C and were cooled to room temperature. Five specimens at each of six aging temperatures were obtained. Five as sintered specimens were also retained. This group of samples is designated as low martensite (LM) due to its lower martensite content. The same steel composition and processing conditions were used to produce another set of specimens with a faster cooling rate to produce specimens with higher martensite content. This group of samples is designated as high martensite (HM) due to its higher martensite content.

Table 1. Nominal Powder Composition of 1% Copper DPPH Alloy (w/o)

C	P	Si	Cr	Ni	Cu	Mn	Mo	Fe
0.013	0.012	0.83	12.11	1.06	0.99	0.07	0.38	Balance

In both the LM and HM groups, specimens from four aging temperatures, as-sintered, 427^{o}C, 538^{o}C, and 593^{o}C were cross-sectioned and polished to a final finish of 0.05 μm silica. Porosity was characterized at three regions in each sample using optical microscopy followed by image analysis (ImageJ, Bethesda, MD). Kalling's Reagent #1 (1.5 g $CuCl_2$, 33 mL HCl, 33 mL ethanol, 33 mL water) was found to be the most effective etchant in distinguishing ferrite and martensite for this material. The specimens were etched by swabbing with the

etchant for four minutes immediately after final polishing. This etchant colors the ferrite phase and etches the martensite [41].

Three microstructurally representative regions of each specimen were imaged using optical microscopy and phase fractions were determined by manually shading the ferritic regions. Image processing by segmentation of the shaded images yielded the ferrite fraction. The martensite fraction was calculated by subtracting the ferrite fraction from the total area excluding the porous regions.

To obtain the local mechanical properties of the microstructure, nanoindentation (Nanoindenter XP-II, Agilent, Santa Clara, CA) was conducted on the ferrite and martensite phases of the LM and HM in as-sintered and aged steel specimens. A continuous stiffness measurement (CSM) technique was used in all experiments [42]. This technique consists of applying a small harmonic, high frequency amplitude during indentation loading, and measuring the contact stiffness of the sample from the displacement response at the excitation frequency. The Young's modulus of the material is then derived from the contact stiffness. The main advantage of the CSM technique is that the modulus and/or hardness can be evaluated as a function of indentation depth. Indentation was conducted with a 3-sided pyramid Berkovich diamond indenter on the etched specimens. Calibration for load and hardness was performed on fused silica. Indentation experiments were conducted under displacement control at a displacement rate of 50 nm/s to an indentation depth of approximately 1000 nm. The hardness and Young's modulus were averaged over a depth range of 600 nm

to 950 nm. Within this range, both the hardness and modulus curves were constant.

All tensile rupture specimens were compacted into a dogbone geometry with an approximate gage length of 38 mm and a total length of 86 mm. Tensile testing for the LM specimens was conducted at a nominal displacement rate of 0.01-0.02 mm/s. The fracture surfaces were examined by scanning electron microscopy (SEM) using a field emission scanning electron microscope (Hitachi S-4700, Hitachi High Technologies America, Inc., Pleasanton, CA).

3.4 Results and Discussion

3.4.1 Microstructure Characterization

Representative optical micrographs of the porosity in LM and HM steels are shown in Fig. 1. Porosity was quantified for specimens processed at the four aging temperatures previously discussed (as sintered, 427°C, 538°C, and 593°C). As Table 2 shows, the average porosities of the LM and HM samples were 24.2% and 27.1%, respectively. Thus, HM samples exhibited slightly higher porosity than the LM samples. The porosities do not vary significantly between aging temperatures (Table 2). The tortuous nature and size of the pores is consistent between the two specimen groups indicating similar pore geometry effects on the tensile behavior.

Table 2. Porosity with Respect to Aging Temperature

Aging Temperature	LM Porosity	HM Porosity
As Sintered	$24.3 \pm 0.4\%$	$26.6 \pm 0.8\%$
427°C	$24.2 \pm 0.9\%$	$27.9 \pm 0.7\%$
538°C	$24.7 \pm 0.9\%$	$27.3 \pm 0.4\%$
593°C	$23.6 \pm 1.1\%$	$26.6 \pm 0.6\%$

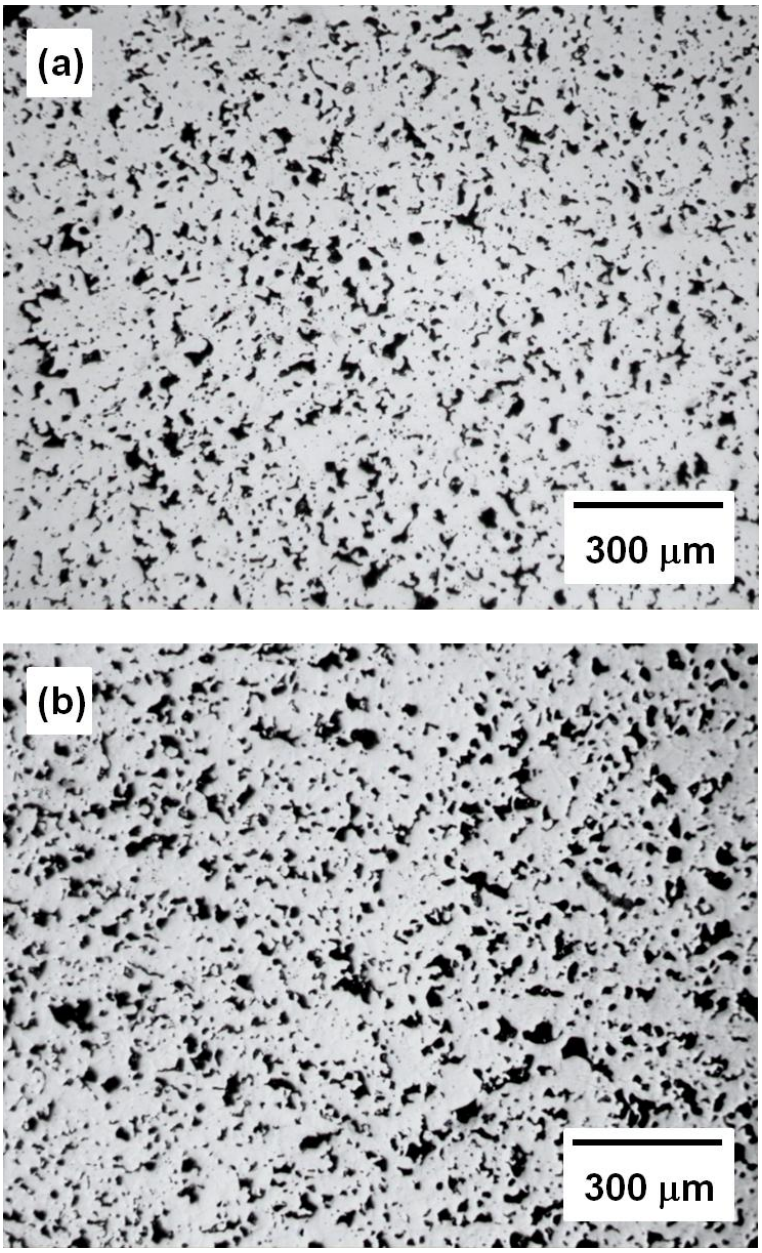

Fig. 1. Optical micrographs of (a) low martensite (LM) and (b) high martensite (HM) as-sintered specimens showing slightly higher porosity for the high martensite group.

Porosity significantly affects the mechanical behavior of steel in two ways. First, the porous areas reduce the load-bearing cross-sectional area of the tensile specimens, thus weakening them to applied loads [2]. Second, irregularly shaped pores act as stress concentrators leading to earlier onset of plasticity and localization of strain [3]. Porosity may also affect the local cooling rates of the material leading to differences in microstructure and mechanical behavior. The small difference in porosity of the LM and HM specimens may not be significant enough to cause the observed large microstructural variations. These are likely a function of the applied macroscopic cooling rate.

The high porosity content of the examined specimens indicates further influence on the steel's properties. Chawla and Deng observed that as density decreased, both the size and the irregularity of the pores increased [43]. Furthermore, at lower densities, the pores were more clustered and distributed along interstices between particles. These observations have two effects. First, irregular pore shape causes high stress concentration at pores which results in localized slip leading to crack initiation [4, 44]. This is expected to increase with increasing hardness of the matrix material. Second, clustering of the pores is representative of inhomogeneous distribution of pores in the material and results in areas of higher than average porosity. Fracture may then occur preferentially in these areas by crack propagation and/or void coalescence between closely neighboring pores. Furthermore, plasticity has been shown to initiate at pore clusters due the higher localized stress intensity associated with these defects [6-8].

The microstructure was studied further by etching the polished surfaces with Kalling's Reagent #1. As shown in Fig. 2, optical microscopy of the etched specimens showed dual phase microstructures containing both ferrite and martensite for both the LM and HM specimens. This microstructure is achieved through the use of specific alloying elements and processing conditions. The nominal steel composition previously presented indicates the presence of ferrite stabilizers (chromium, silicon, and molybdenum) and austenite stabilizers (nickel and copper) in the alloy. These stabilizers alter the ferrite-austenite region on the Fe-C phase diagram and support the development of the dual phase microstructure. Also, at sintering temperature of 1260^{o}C, the alloy is in the two phase ferrite-austenite region due to the low carbon concentration of the steel. Upon rapid cooling, the austenite in the steel transforms to martensite. It is not uncommon for austenite to be retained in the structure upon cooling. However, in low carbon steels, such as that studied here, the amount of retained austenite has been shown to be near zero after quenching due to a martensite finish temperature, M_f, above room temperature [45]. Austenite was not observed in the LM and HM micrographs.

The LM specimens exhibited ferrite and martensite phase fractions of 29% and 81% of the fully dense material, respectively. Significantly lower ferrite and higher martensite fractions of 8% and 92%, respectively, were observed in the HM specimens. The sample naming conventions of LM and HM were derived from these microstructures due to lower and higher martensite fractions between the two groups. Furthermore, the phase fractions were similar for all aging

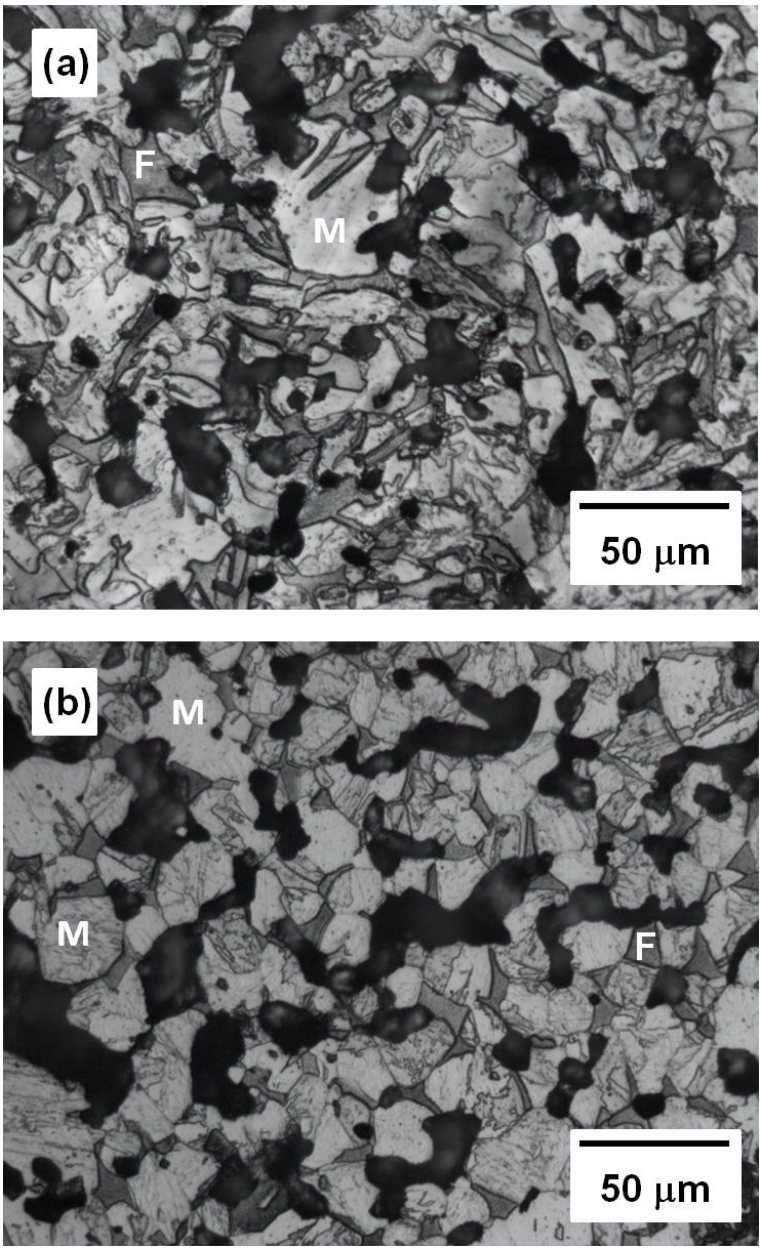

Fig. 2. Optical micrographs of (a) low martensite (LM) and (b) high martensite (HM) specimens etched with Kalling's Reagent No. 1. Ferrite and martensite are labeled with F and M, respectively.

temperatures within the LM and HM groups and optical microscopy showed no significant microstructural differences between the as sintered and aged specimens. This finding is consistent with previous studies of high strength low alloy steel subjected to thermal aging [26]. It should be noted that while the phase fractions do not appear to change with aging temperature, it is possible that local diffusion and relief of residual stresses may be taking place, so that the local mechanical properties might be changing with aging temperature. Precipitates are also presumed to form upon aging but are not detectable by optical microscopy due to its limited resolution. Previous studies showed very small copper precipitates, approximately 10 – 50 nm in size, in steels of similar composition and aging conditions [24, 26].

3.4.2 Mechanical Behavior of the Bulk Steels

Stress-strain curves of the LM and HM specimens show continuous yielding behavior and the lack of defined yield points consistent with dual phase steels (Fig. 3). This behavior has been attributed to high mobile dislocation density in the ferrite near martensite interfaces [10-11] and high residual stresses resulting from the inherent volume expansion associated with the austenite to martensite transformation [11-13]. The austenite-to-martensite volume expansion has been reported to be approximately 2-4% but depends on the carbon concentration of the steel [13, 45]. Upon loading, early plastic flow is observed due to the movement of these mobile dislocations at stresses much lower than required for mobility of restrained dislocations. Plastic flow continues in the ferrite due to its lower yield strength and once this phase is significantly strained,

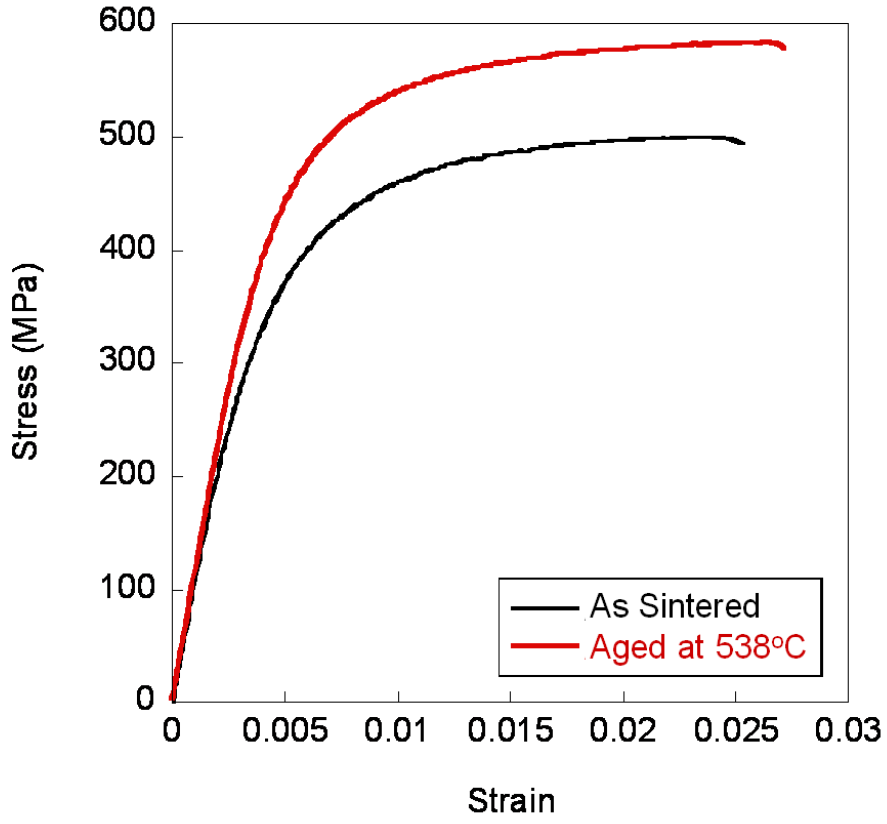

Fig. 3. Example of as sintered and aged high martensite (HM) specimens' stress vs. strain curves showing continuous yielding. Low martensite (LM) specimens also exhibit continuous yielding but are not pictured here.

martensite begins to deform and deformation continues in both phases simultaneously.

The ultimate tensile strength, yield strength, ductility and Young's modulus of the LM and HM specimens are plotted as functions of aging temperature (Fig. 4). The as-sintered conditions are represented at aging temperature zero. For both the LM and HM specimens, the ultimate tensile strengths and yield strengths reach a maximum at an aging temperature of 538^{o}C. These trends presumably result from the precipitation hardening response of copper in the alloys. Up to and including 538^{o}C, fine precipitates form in both the ferrite and martensite resulting from aging treatments. While these precipitates may be carbide and/or nitride based, we focus our attention on the precipitation of copper due to the low carbon and nitrogen contents of this steel. As aging temperatures are increased from the as-sintered condition to 538^{o}C, the copper precipitates grow in size. Dislocation mobility is impeded and the alloy resists deformation and the ultimate tensile and yield strengths increase. At temperatures greater than 538^{o}C, tensile tests indicate softening occurs due to overaging.

Several researchers have investigated the effect of aging on copper-containing steels and have observed similar trends in strength [9, 24-28]. In particular, Dhua et al. [26] evaluated the mechanical behavior of high strength low alloy copper bearing steels which were thermally aged and used transmission electron microscopy (TEM) to explain the strength trends. Similar to the LM and HM specimens studied here, maximum strengths were observed in specimens that were aged at 500^{o}C for 1 hour. TEM showed that as the aging temperature

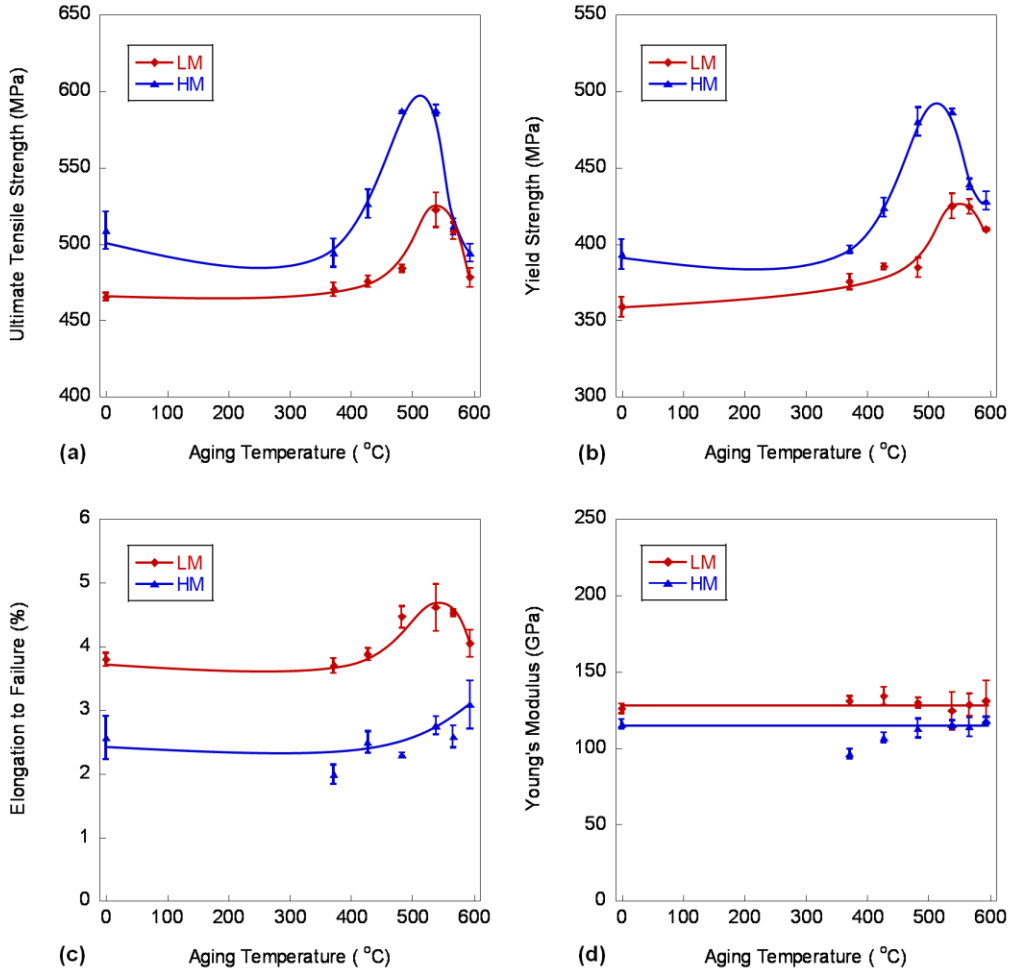

Fig. 4. Effect of thermal aging on (a) ultimate tensile strength, (b) yield strength, (c) elongation to failure, and (d) Young's modulus of low martensite (LM) and high martensite (HM) specimens. Note concurrent increases in strength and ductility with aging.

increased the copper precipitate size also increased from 10-25 nm, in the as quenched state, to 15-30 nm at an aging temperature of 500^{o}C. The increase in precipitate size corresponded to increased strength of the bulk steel. The decrease in strength after aging at 650^{o}C was attributed to coarsened and slightly elongated precipitates, approximately 50 nm in maximum size, which were less effective in hindering dislocation motion. Furthermore, partial recovery of the lath martensite was observed and contributed to softening in the specimens aged at high temperatures.

Carbide precipitation has also been studied in thermally aged steel to elucidate strengthening mechanisms. Jang et al. [34] performed TEM experiments to determine the effect of increasing the Larson-Miller parameter (LMP) on the microstructure of 12% chromium ferritic steel. Though LMP is generally used to quantify creep life, in Jang's study it is simply used to describe the combined effect of time and temperature in thermal aging. As the LMP increased, the carbide precipitate size also increased and very coarse precipitates were often found in the most aged samples, the interparticle spacing increased, and the dislocation density decreased. Since all of these observations are consistent with strength degradation, it is concluded that after a certain time or temperature, overaging occurs and strengthening from precipitates becomes less effective, as in the specimens aged at 593^{o}C. It should be noted that in Jang's study the aging times and temperatures were significantly higher than those used in the current study, and the results are used here to illustrate the carbide

precipitation response in low carbon steels. Furthermore, it is expected that in the currently studied specimens, with their low carbon concentration, that carbide precipitation has less influence on the mechanical behavior than copper precipitation.

Increased strength with aging may also be attributed to reductions in residual internal stresses. At increased temperatures, stress relief is promoted by the tempering of martensite and carbon diffusion. The brittleness of the material is reduced, especially for steels with high martensite content [46]. This is particularly important for PM materials with highly irregular pores because stress relief reduces the notch sensitivity and improves the deformation behavior. In general, tensile strength increases with stress relief due to reductions in brittleness [46]. Grushko et al. [11] also found this occurrence for dual phase steels with high martensite fractions. In our study, some stress relief does occur with aging as shown by increased ductility, as will be discussed later.

By simple composite strengthening theory, it is quite obvious that the higher strengths observed for the HM specimens are due to their higher martensite concentrations. Intuitively, as the fraction of the stronger, harder phase increases, the strength of the composite increases. This is substantiated by previous studies that indicate that the yield and ultimate tensile strengths increase with martensite fraction [13, 15-20]. Furthermore, Erdogan et al. suggested that increases in yield strength may be due to refinements in the microstructure [13]. With their composite microstructure, dual phase steels benefit from grain boundary strengthening between similar and dissimilar phases. Slight differences in the size

and shape of the microconstituents therefore may affect the mechanical behavior. Consistent with these findings, Jiang et al. observed an increase in yield and ultimate tensile strengths with decreasing grain size in dual phase steels [18].

Fig. 4c shows the superimposed plots of the elongation to fracture of the LM and HM specimens with respect to aging temperature. The HM specimens exhibit lower ductility than the LM specimens. Since ferrite imparts ductility in dual phase steels while martensite imparts strength, the lower ductility of the HM specimens is attributed to the higher volume fraction of martensite and hence lower volume fraction of ferrite in this material. Increased continuity of the martensite around the ferrite, as in the HM specimens, may also play a role in the decreased ductility [23]. The coarseness of the martensite phase also contributes to the low ductility for these specimens. Perhaps more importantly, ductility is typically inversely proportional to porosity [47] so the slightly higher porosity of the HM specimens may be a contributing factor to their lower ductility. Higher porosity is known to be more detrimental to ductility than strength. Chawla and Deng observed a significant increase in strain-to-failure with only a slight increase in density of porous sintered steels and attributed this to a narrower and more homogeneous distribution of pores [43]. The ductility of the material may also be influenced by the size distribution, orientation, and degree of clustering of the pores, since the sintered ligaments of the steel control fracture of the material.

Ductility is also shown to increase with aging, though different trends were observed for the LM and HM specimens. Similar to the yield and ultimate tensile strengths, the elongation to fracture exhibits a maximum at 538^{o}C for the

LM group whereas the elongation continually increases with increasing aging temperature for the HM group. This trend results from tempering of the martensite. Upon aging, carbon diffuses out of the martensite reducing the tetragonal shape of the martensite unit cell. Residual stresses in the microconstituents may also be reduced due to contraction of the martensite phase. Due to the low carbon concentration of the steels in this study, the tetragonal distortion of the martensite phase is expected to be lower than that of higher carbon steels and the effect of tempering the martensite may be less profound. Therefore, the ductility is only improved slightly with aging.

Trends in the Young's modulus versus aging temperature are considered insignificant and therefore constant. Higher moduli are observed for the LM specimens. This may be attributed to the lower porosity of the LM group since modulus increases with decreasing porosity [48-49]. Since the moduli of the ferrite and martensite microconstituents are similar, the phase fractions of the LM and HM should not influence the modulus. Therefore, we may neglect the quantities of microconstituents and compare the experimental modulus data to the intrinsic porosities of the two groups. Using the model developed Ramakrishnan and Arunachalam (R-A) [50], the modulus of the fully dense material may be calculated when the modulus is known at various porosity levels. In this model, the interaction of the pores in the material is considered as the intensification of

pressure on a spherical pore's surface. The Young's modulus of the material, E, is given as a function of the fraction of porosity, p [50]:

$$E = E_0\left[\frac{(1-p)^2}{1+\kappa_E p}\right]$$

where E_0 is the modulus of the fully dense material (which is determined by extrapolating the experimental moduli to zero porosity yielding E_0 as 254 GPa), and κ_E is a constant based on the Poisson's ratio, ν_0, of the fully dense steel.

$$\kappa_E = 2 - 3\nu_0$$

It is assumed that the Poisson's ratio for the fully dense steel is 0.3.

Fig. 5 shows a comparison between the R-A prediction and the experimental data. As observed, the experimental data and R-A prediction match reasonably well for the given range of porosity. Since the model is developed on a spherical pore shape, the agreement suggests that pore shape and morphology do not significantly influence the elastic properties of the material.

3.4.3 Local Mechanical Behavior of Microconstituents

To quantify the mechanical properties of the local microconstituents, nanoindentation of the individual phases was performed on the LM and HM samples at the four aging conditions. Nanoindentation is a very advantageous technique, particularly for these types of microstructures, because very small areas can be probed. Use of a Vickers hardness tester might yield multiple phases being sampled and increased contributions from surrounding features. Both the ferrite and martensite illustrated in Fig. 6, were targeted with the Berkovich indenter. Attention was taken to probe the centers of the grains to reduce effects

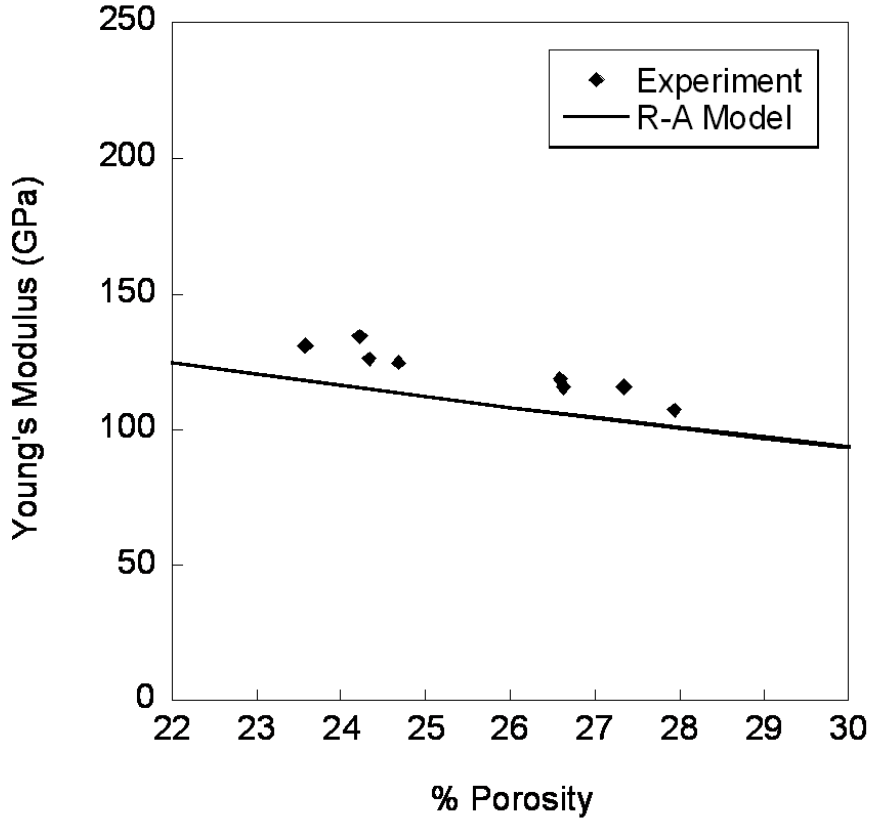

Fig. 5. Young's modulus of P/M steels vs. porosity. The R-A model predicts the experimental data well.

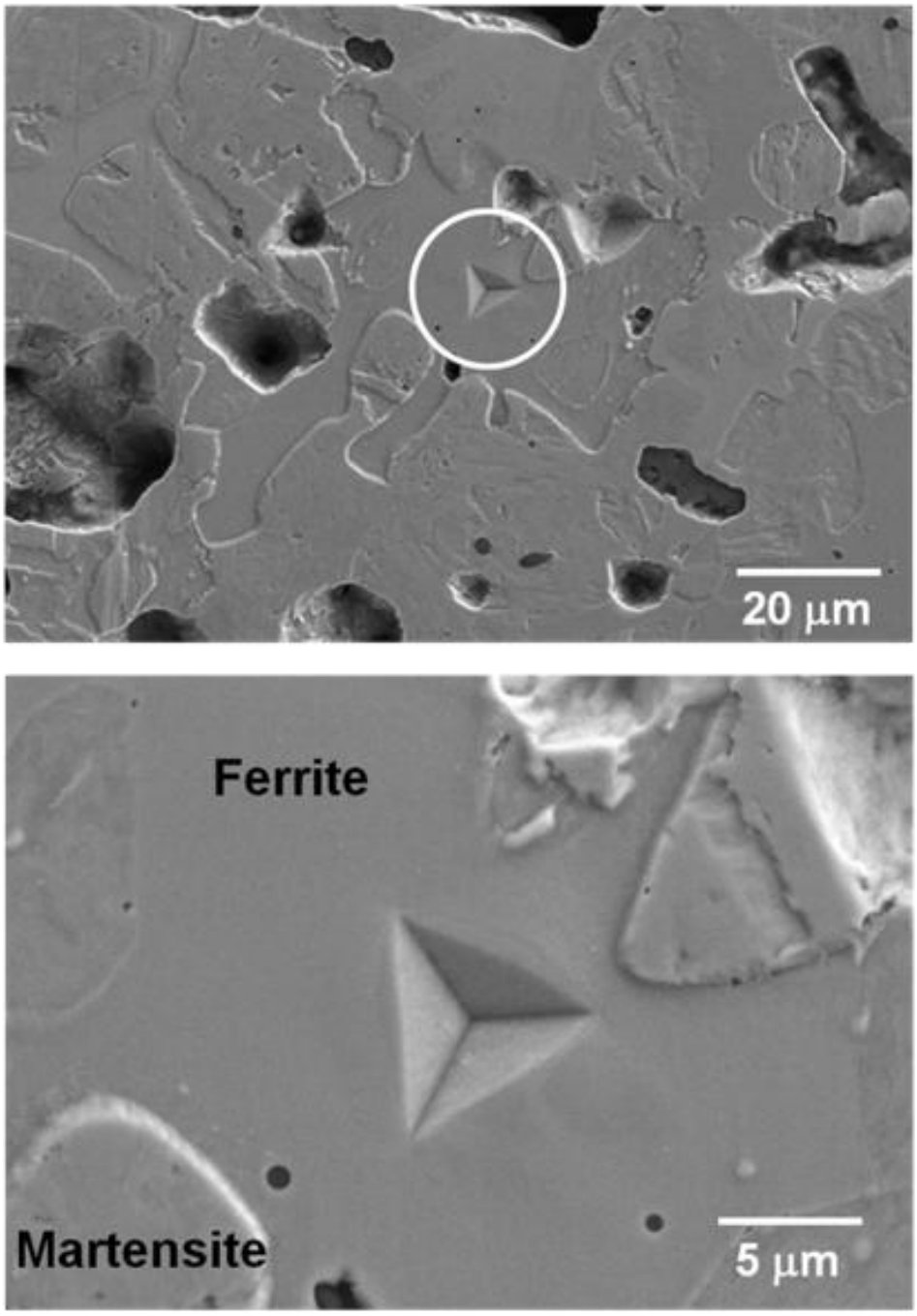

Fig. 6. Example of nanoindentation targeting individual microconstituents on etched steel surface. Ferrite and martensite are denoted by labels.

from the surrounding phases. As expected, Fig. 7 shows that the ferrite had lower hardness than the martensite in all samples. Higher hardness and, for that matter, strength in martensite owe to its high dislocation density and its tetragonal lattice which is supersaturated with interstitial carbon. The HM specimens also had higher ferrite and martensite hardness values than those of the LM specimens in accordance to aging temperature which may be attributed to different cooling rates.

In the LM specimens, the hardness of the ferrite and martensite increased with aging temperature showing maxima at 538^{o}C. The tendency is consistent with trends observed for the yield and ultimate tensile strengths of the bulk composite during tensile testing and suggests that thermal aging influences the mechanical properties of both the ferrite and martensite. Furthermore, these results indicate both ferrite and martensite contribute to overall strengthening in the composite for the LM material of relatively high ferrite phase fraction of 29% Nanoindentation results from the HM specimens exhibited the same trend in which the maximum hardness was observed at 538^{o}C for martensite, but no significant maximum was observed in the hardness of the ferrite. However, aging did increase the ferrite hardness when compared to the as-sintered condition.

While tensile testing showed strengthening behavior of the bulk LM and HM composites, nanoindentation of the ferrite and martensite constituents shed light on the microstructural mechanism. It is shown that both ferrite and martensite are strengthened with aging and therefore both contribute to

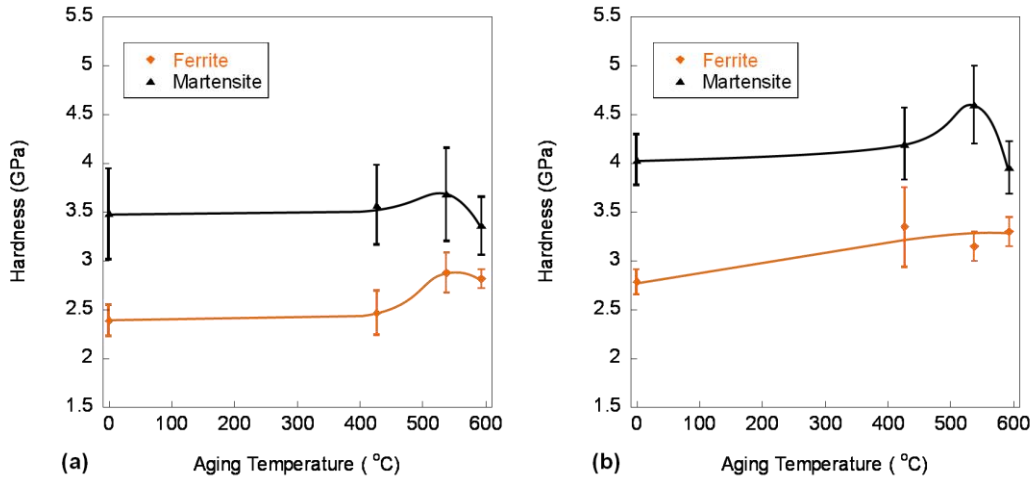

Fig. 7. Effect of thermal aging on nanohardness of ferrite and martensite in (a) low martensite (LM) and (b) high martensite (HM) specimens. Note increased hardness of both microconstituents with aging.

strengthening of the bulk LM and LM and HM composites, though strengthening from the martensite may be dominant due to its much higher phase fraction.

Several mechanisms are at work here. As previously discussed, aging causes the supersaturated solution to precipitate into small intermetallic particles. The particles strengthen the metal matrix through mechanisms such as Orowan bowing that make dislocation motion difficult [29]. Since precipitates in the matrix are exceedingly smaller than the indentation volume currently used, the nanoindentation results include contributions from both the matrix and its precipitates. Increases in hardness with aging suggest that precipitation hardening occurs in both the ferrite and martensite microconstituents and the most effective precipitation response is found in specimens aged at 538^{o}C. At higher temperatures, overaging occurs in which precipitates have grown large enough to allow dislocations to bend and pass between adjacent particles, corresponding to a decrease in hardness. Precipitate growth also results in increased interparticle spacing which contributes to this softening [29]. Strengthening of the ferrite phase has also previously been attributed to the grain size and solid solution hardening from the alloying elements [16, 51]. The latter is more plausible in this case due to no apparent grain size differences between aging temperatures in the LM and HM specimens. Lastly, tempering of the martensite occurs upon aging which relieves residual stresses, results in short-range diffusion, and contributes to enhancements in strength and ductility. At higher temperatures, temper softening may be observed due to rearrangement of carbon atoms and recovery of dislocation structures [35].

Many nanoindentation studies of aged steel have been performed and found that the hardness of martensite decreases with thermal aging due to degradation of the matrix strength and increased tempering of martensite [34-35, 37-40]. This is in direct contradiction to the current study which generally found increased nanohardness with thermal aging. This difference may be explained by the composition of the steels. The current specimens contain approximate 1% copper which, as previously explained, forms intermetallic precipitates that precipitation harden the material. In this way, this steel is unique in that two competing processes are occurring: precipitation hardening and tempering of martensite. Precipitation hardening elements such as copper were omitted from the previously studied materials and therefore the materials did not benefit from strengthening induced by precipitation hardening. Instead this response was limited to the precipitation of carbides and nitrides, of which elemental concentrations were low.

Hernandez et al. [39] used nanoindentation to characterize the heat affected zone of a resistance spot welded wrought dual phase steel. They found that as the distance from the fusion zone increased, the hardness of the martensite increased while the ferrite hardness remained relatively constant. Simulated temperature projections show an inverse logarithmic relationship between temperature and distance from the weld such that as the distance increases, the thermal exposure decreases. These results are consistent with the aforementioned studies that show decreased hardness with increased temperature. The decreased nanohardness of martensite was attributed to increased tempering due to the

observations of more broken martensitic microstructures with the presence of sub-micron particles resulting from the nucleation and growth of carbides. As these carbides form, the remaining martensitic matrix is depleted of carbon and the hardness decreases. In the current study, although the carbon content is similar, this tempered appearance of martensite is not immediately apparent from optical micrographs. Hernandez et al also found that the mechanical behavior of ferrite remained relatively constant with only a slight decrease in nanohardness with increased thermal exposure which is in contrast with the currently studied specimens that showed increased nanohardness with temperature. This may be due to differences in the compositions of the steels since Hernandez's steel did not contain considerable amounts of solid solution hardening elements such as silicon, which promotes hardness in ferrite [16, 51]. Furthermore, this alloy did not include copper or other precipitation hardening elements and therefore neither the martensite nor the ferrite benefited from the precipitation hardening response observed in the current specimens.

As expected, the Young's moduli for the ferrite and martensite were similar over the various aging temperatures (Fig. 8), and the LM and HM specimens exhibited similar moduli. As previously explained, the bulk material's modulus from tensile testing is dependent upon porosity. That is, as the porosity increases the modulus decreases. This is not a factor in the nanoindentation modulus experiments because the small areas which were probed by the indenter were free from voids and thus considered fully dense.

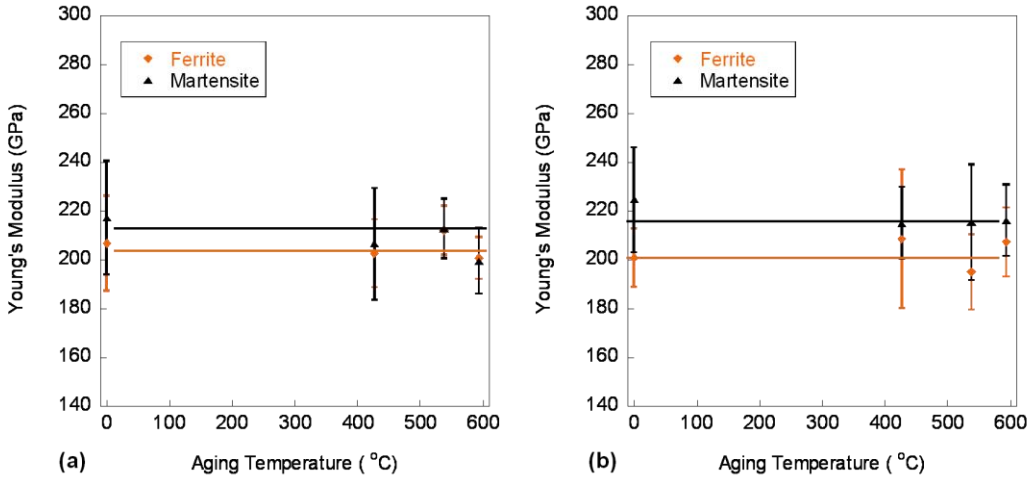

Fig. 8. Effect of thermal aging on Young's modulus of ferrite and martensite in (a) low martensite (LM) and (b) high martensite (HM) specimens showing similar values for ferrite and martensite. No significant differences in modulus are observed with aging.

3.4.4 *Fractographic Analysis*

Fig. 9 shows representative scanning electron micrographs of the fractured surfaces of the as sintered and aged at 538^{o}C LM and HM specimens. Micrographs of the fracture surfaces of the tensile specimens revealed evidence of ductile rupture in the form of void nucleation and growth at second phase particles or microstructural interfaces. Spherical inclusions of various sizes were noted in the dimples and identified as silica through energy-dispersive x-ray spectroscopy (EDS). Some elongated inclusions were also observed suggesting partial coherency of the particles with the steel matrix. Silicon is commonly used in steel to achieve solid solution hardening [16] and to promote carbon migration from ferrite to austenite [52] which transforms to martensite upon cooling. The evidence of silica particulates on the fracture surface indicates that both the LM and HM materials are strengthened by solid solution hardening. Efforts were taken to characterize the size distribution of the silica inclusions but no significant trends were observed. Adequate analysis would require significant inclusion populations. Minimal areas of cleavage were also detected, but the primary rupture was ductile in nature for the as sintered and aged specimens. Ductile rupture is expected in the ferrite phase due to its low hardness and superior ductility. Due to the low carbon content of these steels and tempering from aging, it is reasonable to anticipate ductile rupture in the martensite as well. In fact, plastic deformation of martensite has been observed in previous studies of low carbon dual phase steels of moderate martensite content of greater than 41% [20, 53]. Both the LM and HM specimens have martensite volume fractions

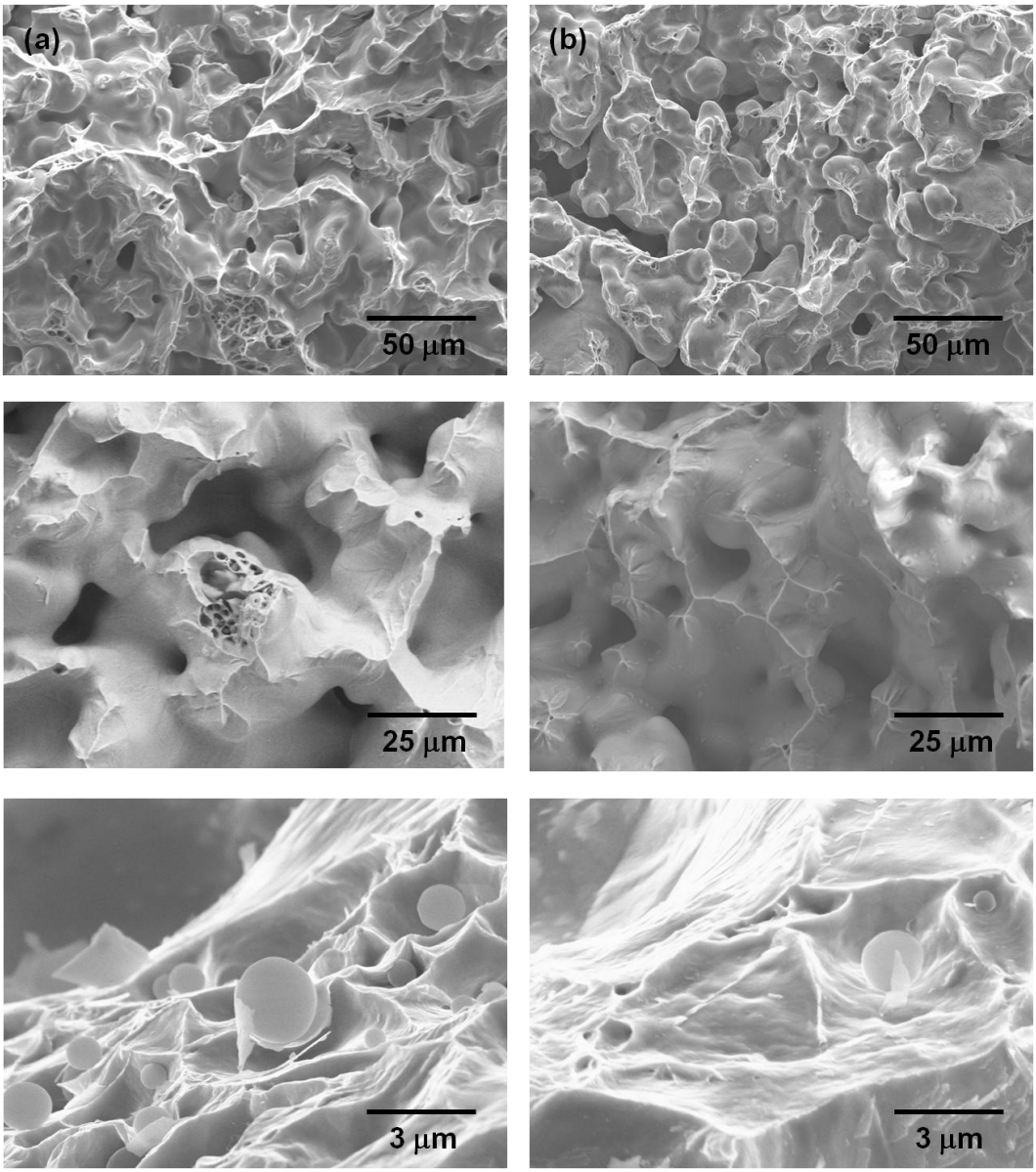

Fig. 9. Fracture surfaces of (a) low martensite (LM) and (b) high martensite (HM) specimens showing ductile rupture in the form of void nucleation and growth at second phase silica particles and microstructural interfaces. Internal necking of the interpore matrix is observed.

higher than this amount, so martensite plasticity is expected in all of the specimens examined here. Furthermore, no apparent differences were noted on the fracture surfaces of the LM and HM specimens. Based on the factors examined in this study, the fractographic analyses suggest that increased martensite concentration does not affect the macroscopic ductile fracture of these alloys.

In PM materials, fracture is primarily controlled by porosity due to reduced load bearing cross-sectional area and the stress concentration effect of irregularly shaped pores. When the material is plastically strained, internal necking of the interpore matrix occurs and pores grow. The area fraction of porosity, as observed in planar projections of the fracture surface, increases due to strain induced pore growth in porous materials thus reducing the effective load bearing cross-section [2]. Furthermore, since pores are randomly spaced, areas of higher than average porosity may exist and cause shear localization in the matrix. Preferential fracture will then occur on shorter interligament paths. Depending on the pore shape irregularity and matrix properties, microcracks may also initiate at pores [4-6] and propagate into the matrix either by cleavage or ductile deformation until they reach an obstacle, another microcrack, or a free surface such as another pore.

Fracture mechanisms similar to those of wrought materials may also be considered in the dense interpore matrix of sintered materials. Many studies have examined the strain distribution between phases in dual phase steels to elucidate the damage mechanism [54-58]. Chawla et al found that in dual phase steels

consisting primarily of ferrite and martensite microconstituent, fracture occurs preferentially at ferrite-martensite interfaces oriented perpendicularly to the loading axis [54]. And that these interfaces have larger discontinuities in mechanical properties than ferrite-inclusion interfaces. Furthermore, microvoids still form at inclusions but later than those formed at the microconstituent interfaces. In agreement with Chawla, Shen et al. [55] observed that shearing occurs at the martensite-ferrite interfaces and strain is transferred from the ferrite to the martensite only after the ferrite is significantly strained. In a study of a dual phase steels intercritically annealed at varying temperatures, Ray also found decohesion at the ferrite-martensite interfaces but also observed fracture in the martensite, crack formation in the ferrite adjacent to sharp martensite corners, and decohesion around inclusions and concluded that no single fracture mechanism exists for dual phase steels [59]. It should be noted that these materials were not subjected to thermal aging and thus the martensite was untempered. In the current study, brittle fracture of the martensite is not expected due to its tempered microstructure and improved ductility. The tempering may also increase the probability of ductile deformation in the martensite as well as the ferrite.

3.5 Conclusions

In this study, we examined the microstructure and mechanical behavior of a PM dual phase precipitation hardened stainless steel and drew the following conclusions:

- Higher porosity and volume fraction of martensite were observed for the HM specimens compared to the LM specimens. No significant microstructural differences were noted with aging in any specimens.
- The HM specimens exhibited higher ultimate tensile strength and yield strength due to increased conventional composite strengthening owing to their increased martensite volume fraction. The HM specimens exhibited lower ductility due to the lower ferrite fraction, increased continuity of the martensite around the ferrite, and higher porosity.
- The yield and ultimate tensile strengths were also observed to increase with increased aging temperature reaching maxima at 538^{o}C. This behavior is attributed to precipitation hardening from the presence of copper and stress relief from carbon diffusion and tempering of the martensite. At higher temperatures, overaging occurs in which precipitates coarsen and the strength decreases. The ductility was also observed to increase slightly with aging due to tempering of the martensite.
- The Young's modulus of the HM specimens was lower than the LM specimens due to increased porosity. The Young's modulus of the fully dense material, which was determined from extrapolation of the experimental data, agreed very well with the theoretical value obtained using the R-A model [50], suggesting little influence of pore shape and morphology on the elastic properties of the material.
- Nanoindentation of the microconstituents showed higher hardness for martensite than ferrite in all cases, owing to martensite's high dislocation

density and tetragonal lattice supersaturated with carbon. The HM specimens demonstrated higher hardness values for both the martensite and ferrite.

- Both the martensite and ferrite hardness values were shown to increase with increased aging temperature and in many cases showed peak hardness at 538^{o}C which is consistent with bulk tensile test results. Since precipitates in the matrix are exceedingly smaller than the indentation volume currently used, the nanoindentation results include contributions from both the matrix and its precipitates and show that both the ferrite and martensite benefit from precipitation hardening. Therefore, both microconstituents contribute to the increased strength of the bulk steel with aging as observed in tensile tests.
- Micrographs of the fracture surfaces of the tensile specimens revealed evidence of ductile rupture in the form of void nucleation and growth at second phase particles or microstructural interfaces. Volume fraction of martensite was not determined to cause significant differences in the rupture mechanism.

3.6 References

1. Introducing PM, Available: www.mpif.org
2. R.J. Boucier, D.A. Koss, R.E. Smelser, O. Richmond, Acta Metall. 34 (12) (1986) 2443-2453.
3. G. Straffelini, Powder Metallurgy 48 (2) (2005) 189-192.
4. J. Holmes, R.A. Queeney, Powder Metall 28 (1985) 231.
5. H.E. Exner, D. Pohl, Powder Metall Intl 10 (1978) 193-196.
6. X. Deng, G.B. Piotrowski, J.J. Williams, N. Chawla, Intl J of Fatigue 27 (2005) 1233-1243.

7. A. Hadrboletz, B. Weiss, Intl Mater Rev 42 (1997) 1-44.

8. S.J. Polasik, J.J. Williams, N. Chawla, Metall Mater Trans A 33A (2002) 73.

9. C.T. Schade, T.F. Murphy, A. Lawley and R. Doherty, Intl J Powder Metall 45 (1) (2009) 38-46.

10. H.J. Klaar, I.A. El-Sesy, A.H.A. Hussein, Steel Research, 61 (2) (1990) 85-92.

11. B. Grushko, B.Z. Weiss, Scripta Metall 23 (1989) 865-870.

12. D.K. Matlock, G. Krauss, L. Ramos, and G.S. Huppi, A Correlation of Processing Variables with Deformation Behavior of Dual-Phase Steels, in *Structure and Properties of Dual-Phase Steels*, American Institute of Mining, Metallurgical, and Petroleum Engineers, 1979, 62-90.

13. M. Erdogan, R. Priestner, Mater Sci and Tech 15 (1999) 1273-1284.

14. M.S. Rashid, Annual Review of Materials Science, 11 (1981) 245-266.

15. I. Tamura, Y. Tomata, A. Okao, Y. Yamaoha, H. Ozawa, S. Kaotoni, Trans Iron Steel Inst Jpn 13 (1973) 283-292.

16. G.R. Speich, R.L. Miller, Mechanical Properties of Ferrite-Martensite Steels, in *Structure and Properties of Dual-Phase Steels*, American Institute of Mining, Metallurgical, and Petroleum Engineers, 1979, 145-182.

17. S. Gunduz, B. Demir, R. Kacar. Ironmaking and Steelmaking 35 (1) (2008) 63-68.

18. Z. Jiang, Z. Guan, J. Lian, Mater Sci and Eng A 190 (1995) 55-64.

19. A. Gural, S. Tekeli, T. Ando, J Mater Sci 41 (2006) 7894-7901.

20. M. Sarwar, R. Priestner, J Mater Sci 31 (1996) 2091-2095.

21. A. Bag, K.K. Ray, E.S. Dwarakadasa, Metall Mater Trans A 30A (1999) 1193-1202.

22. P.H. Chang, A.G. Preban, Acta Metall 35 (5) (1985) 897-903.

23. K. Kocatepe, M. Cerah, M. Erdogan, J Mater Processing Technology 178 (2006) 44-51.

24. S.K. Ghosh, A. Haldar, P.P. Chattopadhyay, J Mater Sci 44 (2009) 580-590.

25. C.N. Hsaio, C.S. Chiou, J.R. Yang, Mater Chem Phys 74 (2002) 134-142.

26. S.K. Dhua, A. Ray, D.S. Sarma, Mater Sci Eng A318 (2001) 197-210.

27. T. Ohmura, K. Sawada, K. Kimura, K. Tsuzaki, Mater Sci Eng A 489 (2008) 85-92.

28. L. Pussegoda and W.R. Tyson, Can. Metall. Q. 23 (1984) 341-347.

29. J. Moon, S. Kim, J. Jang, J. Lee, C. Lee, Mater Sci and Eng A 487 (2008) 552-557.

30. M. Delince, P.J. Jacques, T. Pardoen, Acta Materialia 54 (2006) 3395-3404.

31. T. Ohmura, K. Tsuzaki, S. Matsuoka, Scripta Materialia 45 (2001) 889-894.

32. Y. Choi, W.Y. Choo, D. Kwon, Scripta Materialia 45 (2001) 1401-1406.

33. T.H. Ahn, K.K. Um, J.K. Choi, D.H. Kim, K.H. Oh, M. Kim, H.N. Han, Mater Sci Eng A 523 (2009) 173-177.

34. J. Jang, J Mater Res 22 (1) (2007) 175-185.

35. T. Ohmura, K. Tsuzaki, J Phys D: Appl Phys 41 (2008) 1-6.

36. T.B. Britton, D. Randman, A.J. Wilkinson, J Mater Res 24 (3) (2009) 607-615.

37. T. Ohmura, T. Hara, K. Tsuzaki, Scripta Materialia 49 (2003) 1157-1162.

38. T. Ohmura, K. Tsuzaki, S. Matsuoka, Philosophical Magazine A 82 (10) (2002) 1903-1910.

39. V.H.B. Hernandez, S.K. Panda, Y. Okita, N.Y. Zhou, J Mater Sci 45 (2010) 1638-1647.

40. V.H.B. Hernandez, S.K. Panda, M.L Kuntz, Y. Zhou, Materials Letters 64 (2010) 207-210.

41. G.F. Vander Voort, G.M. Lucas, E.P. Manilova, Metallography and Microstructures of Stainless Steels and Maraging Steels, ASM Handbook 9 (2004) 670-700.

42. W.C. Oliver, G.M. Pharr, J Mater Res 7 (1992) 1564.

43. N. Chawla, X. Deng, Mat Sci Eng A 390 (2005) 98-112.

44. K.M. Vedula, R.W. Heckel, Modern Developments in Powder Metallurgy, Metal Powder Industries Federation, Princeton, NJ, 1981.

45. R.E. Reed-Hill, R. Abbaschian, Physical Metallurgy Principles, 3rd ed. Boston, MA: PWS Publishing Company, 1994.

46. T. Marcu, A. Molinari, G. Straffelini, and S. Berg, International Journal of Powder Metallurgy 40 (3) (2004) 57-64.

47. W.A. Spitzig, R.E. Smelser, O. Richmond, Acta Metall. 36 (5) (1988) 1201-1211.

48. A. Salak, Ferrous Powder Metallurgy, Cambridge International Science Publishing, Cambridge, 1997.

49. N. Chawla, F. Ochoa, V.V. Ganesh, X. Deng, J Mater Sci: Materials in Electronics 15 (2004) 385-388.

50. N. Ramakrishnan, V.S. Arunachalam, J Am Ceram Soc 76 (1993) 2745.

51. Q. Furnemont, M. Kempf, P.J. Jacques, M. Goken, F. Delannay, Materials Science and Engineering A328 (2002) 26-32.

52. P. Abramowitz, R.A. Moll, Metall Trans 1 (1970) 1773-1775.

53. M. Mazinani, W.J. Poole, Metallurgical and Materials Transactions A 38A (2007) 328-339.

54. K.K. Chawla, P.R. Rios, J.R.C. Guimaraes, Journal of Materials Science Letters 2 (1983) 94-98.

55. H.P. Shen, T.C. Lei, J.Z. Liu, Materials Science and Technology 3 (1987) 415-21.

56. F.M. Al-Abbasi, J.A. Nemes, International Journal of Mechanical Sciences 45 (2003) 1449-1465.

57. E. Maire, O. Bouaziz, M. Di Michiel, C. Verdu, Acta Materialia 56 (2008) 4954-4964.

58. X. Sun, K.S. Choi, W.N. Liu, M.A. Khaleel, International Journal of Plasticity 25 (2009) 1888-1909.

59. R.K. Ray, Scripta Metallurgica 18 (1984) 1205-1209.

Chapter 4

MICROCONSTITUENT CHARACTERIZATION BY MICROPILLAR COMPRESSION AND MODELING OF COMPOSITE BEHAVIOR

4.1 Abstract

Micropillar compression has become an attractive method to probe local mechanical behavior. While most micropillar compression work has focused on investigating size effects, we can also use this technique to obtain the constitutive behavior of microscopic phases and constituents. In this study, micropillars of ferrite and martensite were fabricated by focused ion beam (FIB) milling of dual phase precipitation hardened powder metallurgy (PM) stainless steels. Compression testing was conducted using a nanoindenter equipped with a flat punch indenter. The stress-strain curves of the individual microconstituents were obtained. Using a rule of mixtures approach in conjunction with porosity corrections, the mechanical properties of ferrite and martensite were combined to predict the tensile behavior of the bulk material, and reasonable agreement was found for the ultimate tensile strength.

4.2 Introduction

Powder metallurgy (PM) offers many advantages including applicability to a wide variety of alloying systems, production of complex shapes, part to part uniformity, long term performance reliability, minimal scrap loss, and cost effectiveness [1]. Similar to wrought counterparts, PM parts can be produced with a wide variety of microstructures to tailor mechanical behavior and may be heat treated for increased strength and/or wear resistance. However, the early

onset plasticity and localization of strain due to reduction of the load bearing cross-sectional area [2] and the stress concentration effect of angular pores [3] are detrimental to the mechanical properties of porous materials. Several authors have developed relationships to relate strength to porosity [4-11] with limited universal success due to the complex nature of porosity and its effects on the surrounding matrix microstructure.

The increasing demand for high strength PM steels has led to the development of dual phase PM stainless steels [12]. The dual phase steel microstructure consists of both martensite and ferrite microconstituents and is achieved through the use of austenite and ferrite stabilizers in the alloy coupled with specific processing conditions. In addition, low carbon concentration in the alloy is necessary to coincide with the two phase austenite-ferrite region of the Fe-C phase diagram. At high temperatures, the steel is composed of ferrite and austenite but upon cooling, the austenite converts to martensite and the dual phase ferrite-martensite microstructure is achieved. This transformation is known to cause a high dislocation density in the ferrite near martensite-ferrite interfaces [12-14] and high residual stresses [14-16]. Because of the complex microstructures and mechanisms involved, dual phase steels are known to exhibit continuous yielding behavior, high work hardening rate, low yield strength, and high ultimate tensile strength [17]. Dual phase steels also benefit from their composite microstructure in that the martensite imparts strength while ferrite imparts ductility. Hence, the mechanical properties of the steel may be tailored by varying the phase fractions of each constituent. By conventional composite

strengthening, as the fraction of the harder phase, in this case martensite, is increased, the strength of the composite is increased. Several rule of mixtures relationships have been developed to describe the mechanical behavior of the composite microstructure based on the phase fractions and mechanical properties of the microconstituents [18-20].

Understanding the contributions of the individual microconstituents to the mechanical behavior of dual phase steels has proven difficult due to inability to obtain accurate constitutive relationships of each individual constituent. The properties of martensite or ferrite in bulk form are not representative of their behavior at the microscale. Conventional nanoindentation using a sharp tip Berkovich indenter has been used to probe the local mechanical properties of dual phase steels [21-24] but is limited to the determination of the Young's modulus and hardness of the microconstituents. Due to confinement of plastic deformation to a very small volume, non-uniform strain and stress distributions result during indentation. So-called indentation size effects are attributed to these strain gradients as addressed by strain gradient theory [25]. Furthermore, contributions from surrounding features, such as mutual constraint between two phases or grain boundary effects, cannot be removed from conventional nanoindentation experiments. Novel and creative techniques must be used to quantify the constitutive behavior of individual microconstituents.

Micropillar compression of microsized pillars is a promising technique for obtaining the stress-strain behavior at small-length scales. The technique consists of the fabrication of free-standing pillars in the micron to nanometer scale, which

can be isolated to individual phases, followed by compression using a nanoindenter with a flat punch. For the most part, this technique has been used to study size effects on mechanical properties [26-33] of single crystal materials. In addition, Jiang and Chawla [34] have used the technique to obtain the constitutive behavior of intermetallic phases formed in Sn-based alloys. Most applicable to the current study, Pouchon et al. [35] performed micropillar compression studies of irradiated oxide dispersion strengthened (ODS) ferritic steel alloys and compared micropillar compression results to those of tensile tests with reasonable success.

In this study, micropillar compression was employed to determine the mechanical properties of individual microconstituents in a PM-processed dual phase steel. Furthermore, this testing was conducted on both as-sintered and thermally aged specimens to gain an understanding of the effect of aging on deformation behavior. Using a modified rule-of-mixtures approach for dual phase steels, the composite behavior of the steel was quantified. The constitutive behavior of the phases developed from micropillar compression was coupled with existing strength-porosity models from the literature to predict the ultimate tensile strength of the steel. Direct comparisons of the predictions with tensile tests of the bulk dual phase steel were conducted and the correlations were quite good.

4.3 Materials and Experimental Procedure

The specimens used in this study were processed by Hoeganaes Corporation. The nominal composition of the dual phase precipitation hardened (DPPH) steel alloy is shown in Table 3. The powders were mixed with 0.75 w/o

of an organic binder (Acrawax C, Promaplast, Mexico) and compacted at 386 MPa into standard rectangular shapes with gage and total lengths of approximately 38 mm and 86 mm, respectively. The samples were sintered for 30 minutes at 1260^{o}C in hydrogen to a density of 6.60 g/cm^{3}. After cooling, five specimens were aged in 100% nitrogen for 1 hour at a temperature of 538^{o}C and were cooled to room temperature. Five as sintered specimens were also retained. Tensile testing was conducted at a nominal displacement rate of 0.01 mm/s.

Table 3. Nominal Powder Composition of 1% Cu DPPH Alloy (w/o)

C	P	Si	Cr	Ni	Cu	Mn	Mo	Fe
0.013	0.012	0.83	12.11	1.06	0.99	0.07	0.38	Balance

The as-sintered and aged specimens were cross-sectioned and polished to a final 0.05 μm silica finish. The porosity was characterized at three regions in each sample using optical microscopy followed by digital image analysis. Kalling's Reagent #1 (1.5 g $CuCl_2$, 33 mL HCl, 33 mL ethanol, 33 mL water) was used as an etchant to distinguish ferrite and martensite. This etchant colors the ferrite phase and etches the martensite [36]. The specimens were etched by swabbing with the etchant for four minutes immediately after final polishing. Three microstructurally representative regions of each specimen were imaged using optical microscopy and phase fractions were determined by manually shading the ferritic regions. Image processing by segmentation of the shaded images yielded the ferrite fraction. The martensite fraction was calculated by subtracting the ferrite fraction from the total area excluding the porous regions.

Micropillars were fabricated in both the ferrite and martensite phases of the as sintered and aged specimens using a focused ion beam (FEI FIB/SEM Nova 200, Hillsboro, OR). These pillars were fabricated in two steps. First, a rough pillar with a surrounding 20 μm trench was formed using a voltage and current of 30 kV and 5 nA, respectively. The resulting pillar structure was of relatively large diameter (4 μm). A second pass was conducted at a lower current (0.3 nA) and resulted in pillar diameters of ~ 1.5 μm and heights of ~4 μm. The final pillars exhibited a slight taper of approximately 5-6^{o} so the aforementioned pillar diameter is representative of the diameter at the top surface of the pillar. Effort was taken to maintain similar pillar volumes and dimensions for all fabricated pillars. To accomplish this, different milling dimension parameters on the second pass were necessary for the ferrite and martensite phases. The effect of ion beam damage from Ga^{+} ion implantation was assumed negligible since previous studies have estimated it to be no more than 60 nm at 30 kV under normal incidence [30, 37] which is significantly less than the pillar dimensions and compression displacement used here.

The micropillars were compressed using a commercial nanoindenter (Nanoindenter XP-II, Agilent) equipped with a Berkovich three-sided pyramid diamond indenter with a flat tip. This tip had a flat triangular cross-section with a 10 μm side, thus having adequate surface area to accommodate the entire pillar diameter. The formation of the 20 μm trench around the pillars in the previous milling steps prevented the indenter from contacting the surrounding material and allowed for easy location of the pillars. A continuous stiffness measurement

(CSM) technique was used in all experiments [38]. This technique consists of applying a small harmonic, high frequency amplitude during indentation loading, and measuring the contact stiffness of the sample from the displacement response at the excitation frequency. The main advantage of the CSM technique is that the contact stiffness can be measured instantaneously as a function of indentation depth. A displacement of 1000 nm was used for all pillar compression experiments. The resulting load-displacement curves were converted to stress-strain plots by the method of Greer et al. Here it is assumed that plastic volume is conserved upon loading the cylindrical pillar [28]. After deformation, fractographic analysis of the pillars was conducted on the pillars using a dual beam FIB equipped with a scanning electron microscope (SEM).

4.4 Results and Discussion

4.4.1 Microstructure Characterization

Quantitative analysis of pore fraction, as well as phase fractions of ferrite and martensite were conducted. Representative optical micrographs of the steel's porosity are shown in Fig. 10. Porosity levels for the as-sintered and aged (at 538^{o}C) specimens were determined to be 26.6 ± 0.8% and 27.3 ± 0.4%, respectively. Clearly, porosity does not vary significantly with aging temperature. The tortuous nature and size of the pores is also consistent between the two aging conditions. Porosity primarily affects mechanical behavior by reducing the load-bearing cross-sectional area [2] and introducing stress-concentrators at irregularly shaped pores leading to early onset of plasticity and localization of strain [3].

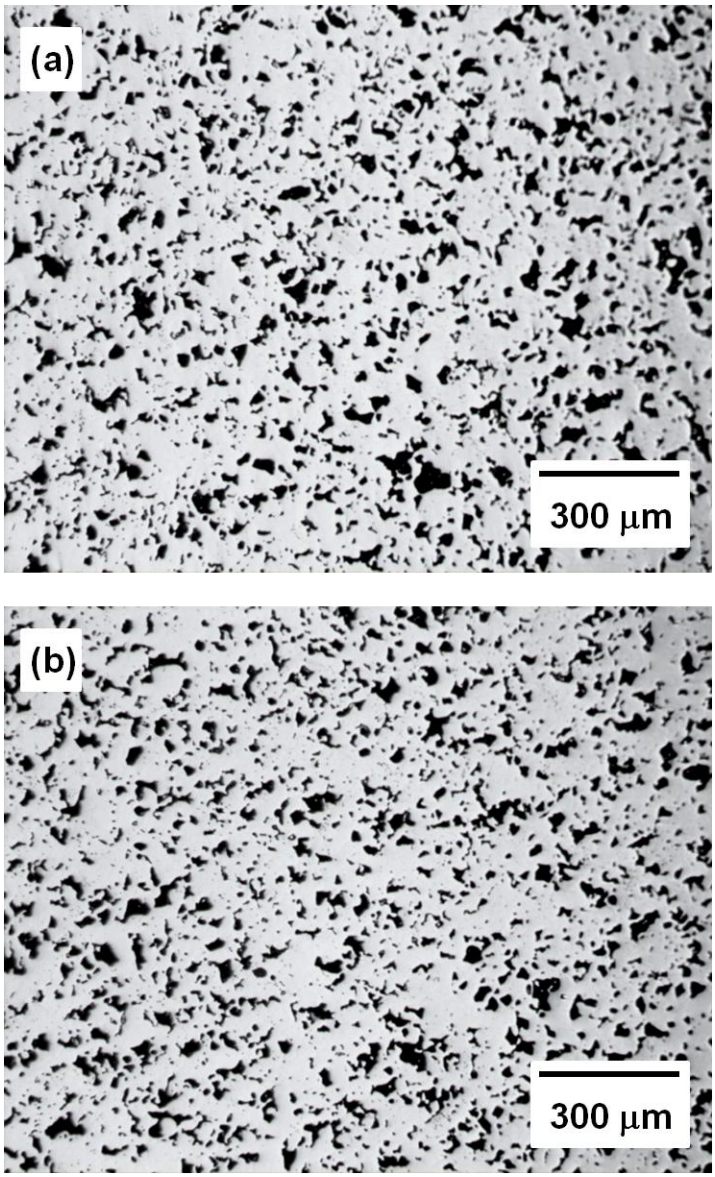

Fig. 10. Optical micrographs showing similar porosity for the (a) As Sintered and (b) Aged at 538°C specimens.

Porosity may also affect the local cooling rates of the material leading to differences in microstructure and mechanical behavior [24].

The microstructure was studied further by etching the polished surfaces. The dual phase microstructures containing both ferrite and martensite, in both the as-sintered and aged specimens, are clearly seen, Fig. 11. This microstructure is achieved through the use of specific alloying elements and processing conditions. The nominal steel composition consists of ferrite stabilizers (chromium, silicon, and molybdenum) and austenite stabilizers (nickel and copper) in the alloy. These stabilizers alter the ferrite-austenite region on the Fe-C phase diagram in support of the development of the dual phase microstructure. Also, at the sintering temperature of 1260^{o}C, the alloy is in the two phase ferrite-austenite region due to the low carbon concentration of the steel. Upon rapid cooling, the austenite in the steel transforms to martensite. It is not uncommon for austenite to be retained in the structure upon cooling. However, in low carbon steels, such as that studied here, the amount of retained austenite has been shown to be near zero after quenching due to a martensite finish temperature, M_f, above room temperature [39]. Austenite was not observed in our microstructural analysis and was assumed to be below the detection limits of typical x-ray diffraction techniques.

The phase fractions of ferrite and martensite content were approximately 8% and 92%, respectively. The measured phase fractions were identical for both as-sintered and aged specimens. Optical microscopy also showed no significant microstructural differences in grain size and shape, tempered martensite

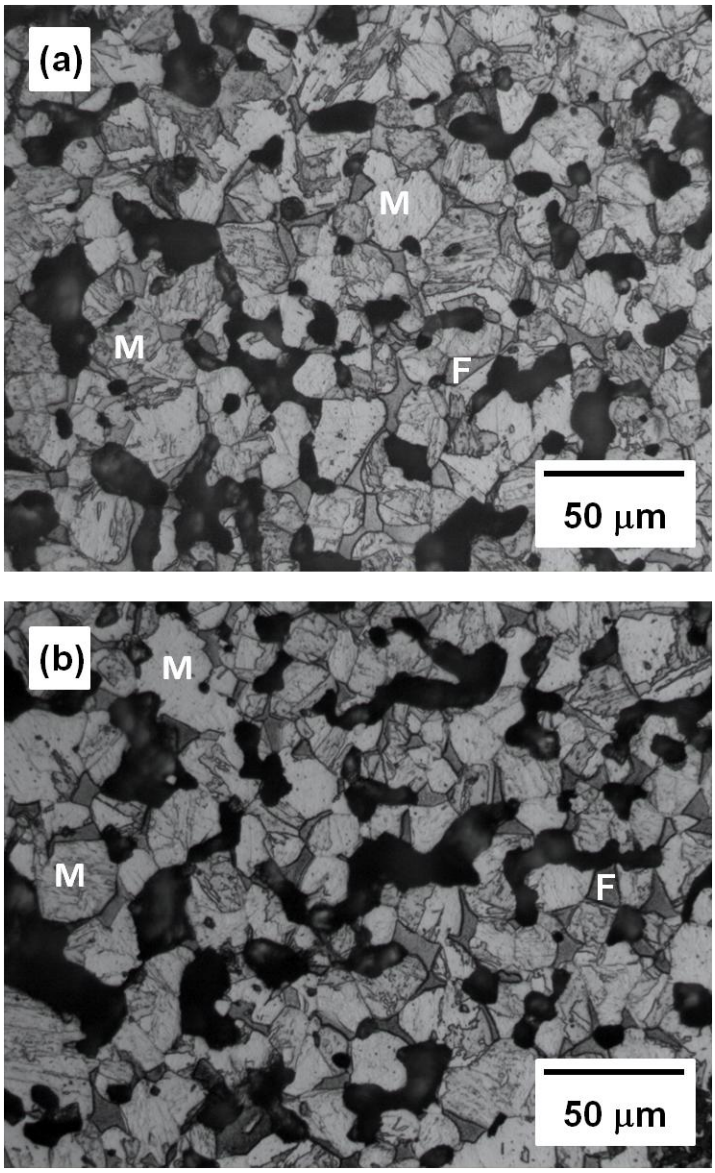

Fig. 11. Optical micrographs of (a) As sintered and (b) Aged at 538^{o}C specimens etched with Kalling's Reagent No. 1. Ferrite and martensite are labeled with F and M, respectively. Note similar phase fractions for as sintered and aged specimens.

appearance, etc., between the as-sintered and aged specimens. This finding is consistent with previous studies of high strength low alloy steel subjected to thermal aging [40]. It should be noted that while the phase fractions do not appear to change with aging temperature, it is possible that local diffusion and relief of residual stresses may be taking place, so that the local mechanical properties might be changing with aging temperature. Precipitates are also presumed to form upon aging but are not detectable by optical microscopy due to its limited resolution. Previous studies showed very small copper precipitates, approximately 10 – 50 nm in size, which were only detectable by transmission electron microscopy, in steels of similar composition and aging conditions [40-41]. Copper precipitates are expected to grow in size with thermal aging of the steel.

4.4.2 Mechanical Behavior of the Bulk Steels

Tensile stress-strain curves of the as-sintered and aged specimens show continuous yielding behavior and the lack of defined yield points consistent with dual phase steels (Fig. 12). This behavior has been attributed to high mobile dislocation density in the ferrite near martensite interfaces [13-14] and high residual stresses resulting from the inherent volume expansion associated with the austenite to martensite transformation [14-16]. Upon loading, early plastic flow is observed due to the movement of these mobile dislocations and flow continues in the ferrite due to its lower yield strength. Once this phase is significantly strained, the martensite begins to deform and deformation continues in both phases simultaneously. Early plastic flow may also result from localization of strain due

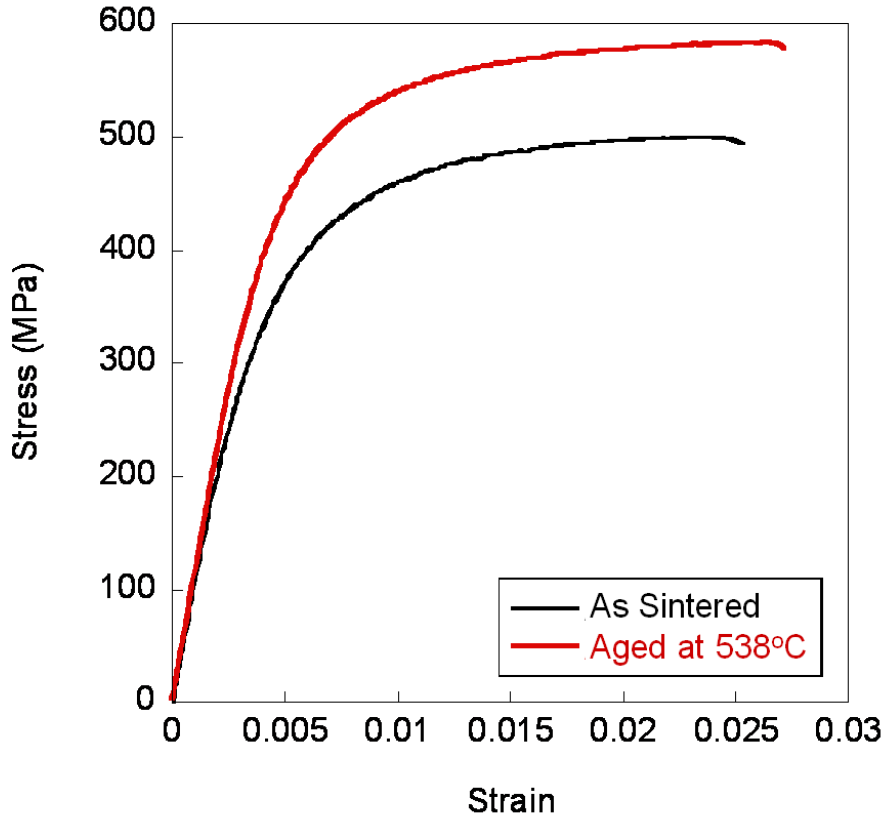

Fig. 12. Example of as sintered and aged specimens' stress vs. strain curves showing continuous yielding and increased strength with aging.

to the irregular pore shape or inhomogeneous pore distribution. Irregular pore shape causes high stress concentration at pores which results in localized slip leading to crack initiation [42-43]. This is expected to increase with increasing hardness of the matrix material. Clustering of the pores is representative of inhomogeneous distribution of pores in the material and results in areas of higher than average porosity at which fracture may then occur preferentially by crack propagation and/or void coalescence between closely neighboring pores. Furthermore, plasticity has been shown to initiate at pore clusters due the higher localized stress intensity associated with these defects [44-46].

The ultimate tensile strengths and yield strengths (as 0.2% offset) of the as-sintered and aged specimens are shown in Table 4. Young's modulus and strain-to-failure were also determined [24] but are beyond the scope of this work and are therefore not discussed here. Increases in both the yield strength and ultimate tensile strength are observed with aging. These trends presumably result from the precipitation hardening response of copper in the alloys. During aging, fine precipitates form in both the ferrite and martensite. We focus our attention on the precipitation of copper due to the low carbon and nitrogen contents of this steel. As aging temperatures are increased from the as-sintered condition to 538^{o}C, the supersaturated solution decomposes and copper precipitates grow in size. Dislocation mobility is impeded and the alloy resists deformation. Reductions in residual internal stresses likely also contribute to increased strength.

Table 4. Tensile Testing of As Sintered and Aged Specimens

Aging Temperature	σ_{UTS} (MPa)	σ_{YS} (MPa)	E (GPa)	Strain-to-Failure (%)
As-sintered	509 ± 12	394 ± 10	116 ± 3	2.6 ± 0.3
538°C	588 ± 4	487 ± 2	116 ± 3	2.8 ± 0.1

4.4.3 Micropillar Compression

Stress-strain plots for the individual microconstituents were obtained by micropillar compression. The top diameter of the pillar was used to calculate the nominal cross-sectional area of the pillars as in previous studies [33, 47]. The strain was calculated as the ratio of the measured displacement to the original pillar height less its plastic compressive displacement (expressed as a percentage). The method of Greer et al. [28] was used to correct the stress-strain curve, whereby the pillars are assumed to be perfectly cylindrical and the volume during plastic deformation is assumed to be conserved during compression. The resulting stress-strain curves are shown in Fig. 13. Two tests for each microconstituent per aging condition were completed. A summary of the tensile properties is shown in Table 5.

Table 5. Yield and Fracture Strengths of Ferrite and Martensite from Micropillar Compression

Aging Temperature	Yield Strength (MPa)		Fracture Strength (MPa)	
	Ferrite	Martensite	Ferrite	Martensite
As-Sintered	569 ± 8	887 ± 53	823 ± 40	1475 ± 143
538°C	610 ± 151	1177 ± 54	808 ± 146	1858 ± 348

As expected, micropillar compression tests show higher strengths for martensite when compared to ferrite. The effect of aging is also examined. The yield strength of ferrite is observed to increase with aging temperature, while the

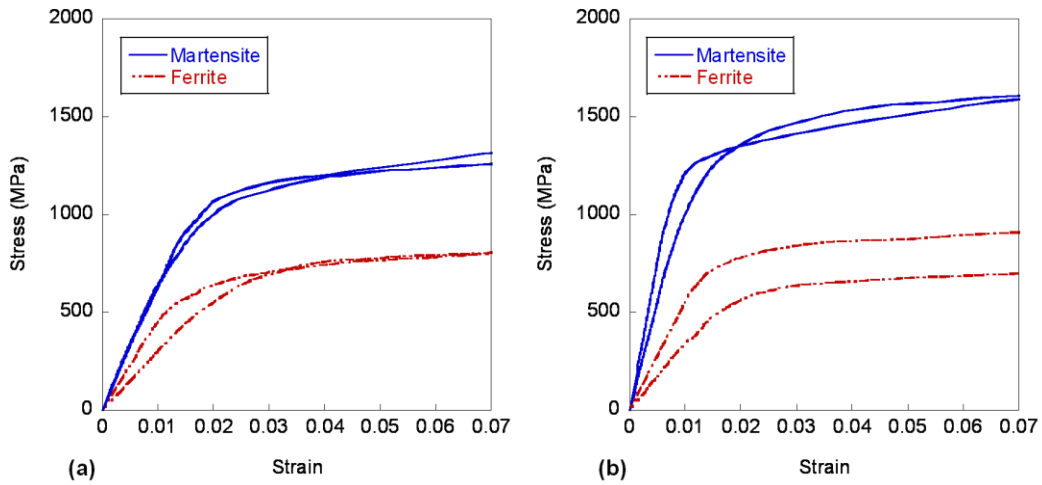

Fig. 13. Stress-strain curves from ferrite and martensite micropillar compression of (a) As sintered and (b) Aged at 538^{o}C specimens. Note increased martensite strength with aging.

fracture strength remains relatively constant. It is arguable that both the yield and fracture strengths of ferrite are within test scatter and therefore may be considered to remain constant with aging. Martensite, however, exhibits both increased yield and fracture strengths with aging which is consistent with results from tensile tests of the composite dual phase bulk specimens. This increased strength with aging is attributed to the growth of copper containing precipitates which hinder dislocation motion by mechanisms such as Orowan bowing [24]. It is therefore concluded that martensite is the primary driver of increased strength with aging in the bulk, especially with its predominate martensite phase fraction of 92%. Micrographs of representative pillars in ferrite and martensite (pre and post-deformation) are shown in Fig. 14. Nearly constant initial volumes and dimensions were maintained for all fabricated pillars. Deformation is observed to occur by crystallographic slip.

Much of the work on micropillar compression has focused on size effects observed in single crystal materials, in which increased strength is noted with decreased pillar size due to dislocation starved conditions [26-29, 31-33]. In the current work, the objective was to obtain the constitutive stress-strain behavior of the individual microconstituents, and not to investigate size effects. As such, the volumes tested here are likely large enough to be in the regime where size effects do not play a role since the current pillar diameter is greater than the critical diameter of approximately 1 μm previously noted [29]. In addition, the steel studied here is not expected to suffer from size effects due to its inherent defect and dislocation density. Pouchon et al. [35], in fact, observed good agreement in

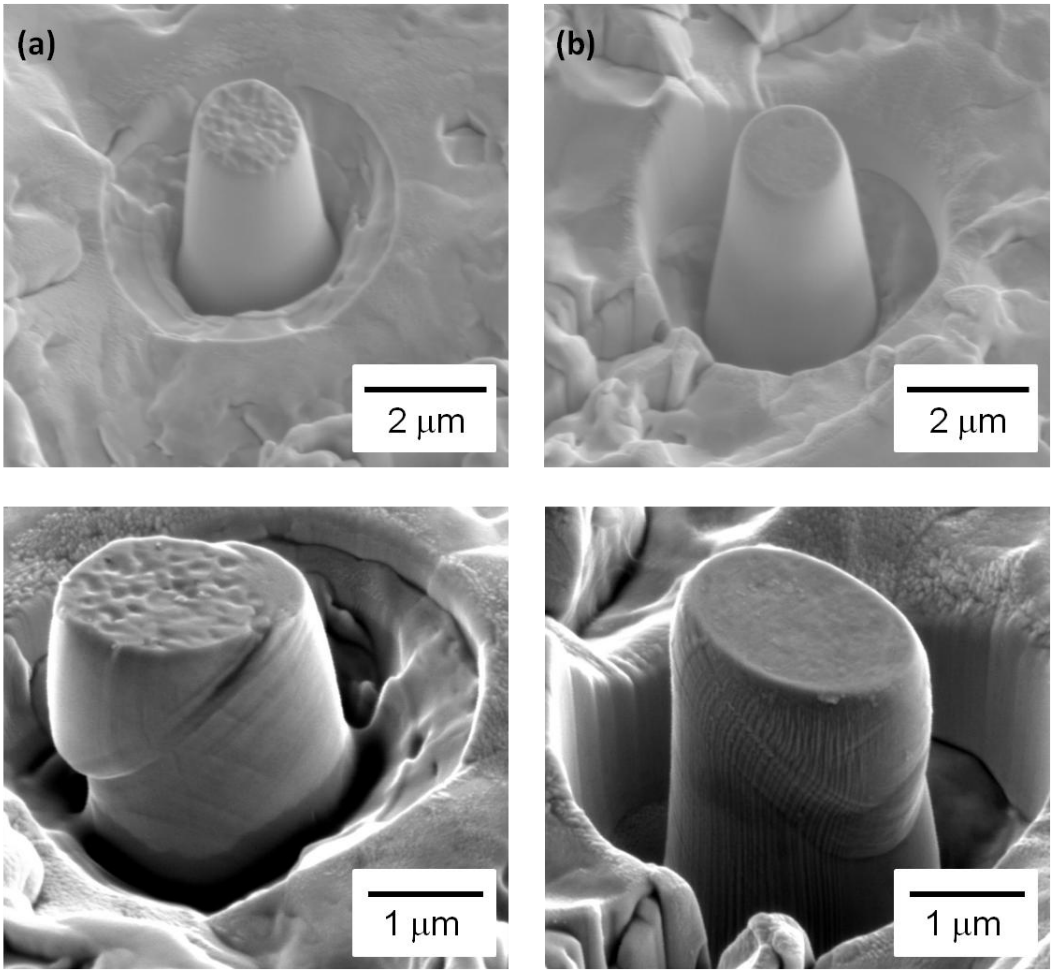

Fig. 14. Scanning electron microscope images of (a) ferrite and (b) martensite pillar pre and post deformation. Note pillar deformation occurs by crystallographic slip.

the yield stresses measured by tensile testing and micropillar compression tests of irradiated ferritic steel and therefore concluded that size effects were not present in the material. This absence of the size effect was attributed to the presence of defects in the material. It should also be noted that Pouchon's pillars were of similar diameter to the pillars investigated here.

4.4.4 Using Stress-Strain Data from Microconstituents to Predict Bulk Behavior

In this section we aim to incorporate the microconstituent stress-strain response from micropillar compression experiments to predict the bulk tensile behavior. It is necessary to apply a rule of mixtures model to translate the microconstituents' properties into composite properties of the bulk steel. Due to the inherent differences in mechanical behavior of the microconstituents, many authors have considered various rule of mixtures relationships to describe the mechanical behavior of dual phase steels of varying phase fraction [18-20]. Speich and Miller [18] worked under the assumption that gross flow in martensite does not occur until the ultimate tensile strength of the ferrite is reached, and therefore the ultimate strength of the composite is represented by:

$$S_u = S_{m,0.2\%} V_m + S_{f,u} V_f$$

where S_u is the ultimate tensile strength of the composite, $S_{m,0.2\%}$ is the 0.2% offset yield strength of martensite, $S_{f,u}$ is the ultimate tensile strength of ferrite, and V_m and V_f are the phase fractions of martensite and ferrite, respectively. This relationship operates under the traditionally held idea that ferrite imparts ductility while martensite imparts strength in dual phase steels. Tamura et al. [19] assumed that deformation in dual phase steels occurs somewhere between

isostrain and isostress conditions and considered that engineering stress and strain are partitioned between the two phases as given by:

$$S = S_f V_f + S_m V_m$$
$$\varepsilon = \varepsilon_f V_f + \varepsilon_m V_m$$

where S_f and S_m are the engineering stresses in ferrite and martensite, respectively, while ε_f and ε_m are the engineering strains. Since it is unlikely that the strains in the ferrite and martensite will be in a fixed ratio throughout deformation due to their differing mechanical properties, Rios et al. [20] expanded on this idea and developed a relationship to further describe the partitioning between the phases. It was assumed that the steel deforms uniformly up to the onset of plasticity due to similar elastic moduli of the microconstituents, after which variations in stresses in the ferrite and martensite are approximated to behave in a linear fashion. Thus, the stress in the martensite, S_m, is given by:

$$S_m = S_{f,y} \frac{S_{f,u} - S_{m,0.2}}{S_{f,u} - S_{f,y}} + S_f \frac{S_{m,0.2} - S_{f,y}}{S_{f,u} - S_{f,y}}$$

Where $S_{f,y}$ is the yield stress of ferrite. Therefore, if the stress-strain behavior of the ferrite and martensite are known, the stress-strain curve of the composite dual phase steel may be calculated by solving for S_m and substituting into Tamura's relationship for stress of the steel. The strains from the ferrite and martensite compression tests are used in Tamura's equation for total strain. In the current study, it is expected that the ferrite fraction is too low to solely support early deformation and thus ferrite and martensite will simultaneously deform. Therefore, we utilize a conventional rule of mixtures model, like that given by

Tamura, to obtain the fracture strengths and stress-strain curves for the composite microstructure (Fig 15).

Using the ferrite and martensite fracture strengths from micropillar compression (Table 5), the fracture strengths of the as-sintered and thermally aged dual phase steels were found to be 1420 MPa and 1770 MPa, respectively. These strengths are representative of the fully dense composite microstructure since all pillars are assumed to be non-porous.

The bulk tensile tests are inclusive of the steel's porosity (~27%) and therefore the aforementioned rule of mixtures results must be adjusted for porosity since porosity significantly affects strength. Several relationships for strength as a function of porosity have previously been developed but with difficulty due to oversimplification of pore shape, morphology, and distribution. These relationships are also confounded by the effect of porosity on microstructure. As a result, it is nearly impossible to develop a universal strength-porosity equation that is applicable to all materials. We therefore present a review of select strength-porosity relationships for sintered iron compacts from the literature. For all equations, σ is the tensile strength of the porous material, σ_0 is the tensile strength of the fully dense material, and p is the fraction of porosity. Other constants are explained below.

Salak et al. [4] evaluated the ultimate tensile strength-porosity relationship of over 800 iron compacts from his own experiments and those in the literature and developed an equation based on a best fit line of experimental data. In doing so, a wide variety of pore sizes and shapes as well as microstructures were

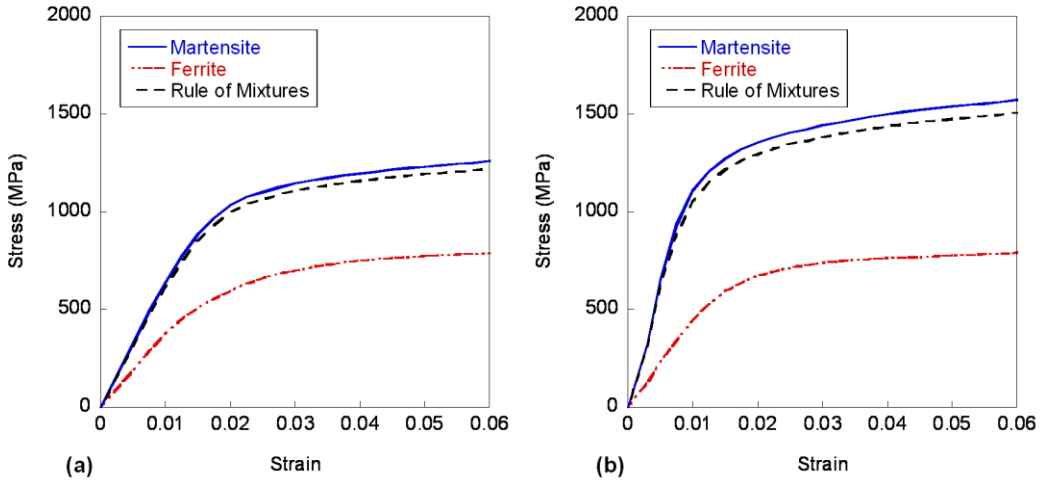

Fig. 15. Average ferrite and martensite curves from micropillar compression with calculated Rule of Mixtures curves using 8% ferrite and 92% martensite of (a) As sintered and (b) Aged at 538^{o}C specimens.

examined. He found that this best fit line was solved by using a stress intensity factor of 4.3 and reported the ultimate tensile strength of porous iron compacts as follows:

$$\sigma = \sigma_0 e^{-4.3p}$$

Due to wide variation in strength amongst similar porosity levels, the relationship is only representative of the mean best fit and at best provides an approximation of the predicted strength. Therefore, the stress intensity factor is expected to vary amongst different materials depending on the nature of their porosity. A generalized form of this relationship is also reported in the literature without specifying an absolute value for the stress intensity factor, K [5, 10], though other empirical studies of sintered steels have found this value to be 10 [10]. The wide variation in the stress concentration factor indicates that this factor is a function of pore shape and pore size in addition to total porosity.

Troshchenko [6] considered the effect of porosity in reducing the load bearing cross-sectional area and formulated the following equation to predict the strength of porous sintered materials,

$$\sigma = \sigma_0 \frac{(1 - ap)}{(1 + \beta a)}$$

where β describes the non-uniformity of the stress distribution across the cross-section and a represents the surface area of the pores. For sintered iron powders, Troshchenko found good correlation to experimental data using β as 2 and a as1.5 times the fractional porosity (a=1.5p).

Haynes [7] developed a strength-porosity relationship by taking into account stress-intensification by pores and implementing a factor, b, which is dependent upon a pore sensitivity factor, K_p.

$$\sigma = \sigma_0 \frac{(1-p)}{1+bp}$$

$$b = a(K_p - 1)$$

Experimental data for a variety of steels most closely matched theoretical values using b values between 2 and 5, where b increases with decreasing ductility. Again, only a range of strengths was able to be predicted due to variation in mechanical properties of various steels. For the current study of aged steel, where ductility is expected to be low, we therefore use b equal to 4 as a reference.

Fleck and Smith [8] investigated both variable morphology and simple brick models to incorporate the effect of microstructure into a strength-porosity relationship. We focus our attention on the simple brick model here. In this model, pores and particles may be represented by a randomly arranged layered array of cubes where the probability of the existence of a pore is given by $p^{2/3}$ and the probability of the existence of particle is $(1-p^{2/3})$. Furthermore, the probability of the failure plane occurring between two solid particles is $(1-p^{2/3})^2$ and the strength of the sintered material is proportional to this component as follows.

$$\sigma = \sigma_0 (1 - p^{2/3})^2$$

Though the stress concentrating effect due to pore geometry is ignored, Fleck found reasonable agreement to experimental values of sintered steel by applying this model.

These strength-porosity models were applied to the fracture strengths from the aforementioned rule of mixtures analyses of the micropillar compression of ferrite and martensite. The resulting composite strengths which are, thus, inclusive of porosity were then compared to the ultimate tensile strengths from tensile tests of the bulk composite steel and reasonable agreement was found (Table 6). This agreement validates the approach of micropillar compression to determine the strength of individual microconstituents as a basis of predicting the overall material behavior.

Table 6. Comparison of Ultimate Tensile Strength (MPa) of Bulk Steel from Tensile Testing and Calculated Fracture Strength (MPa) of Composite from Micropillar Compression

	As-Sintered	Aged at 538^{o}C
Tensile Test	509	588
Salak Model [4]	445	554
Troshchenko Model [6]	467	581
Haynes et al. Model [7]	498	621
Fleck and Smith Model [8]	481	600

Variations in the tensile experimental data and the results from the application of the various porosity-strength relationships may be explained by oversimplifications in the models regarding pore size, shape, orientation, and distribution as well as the non-uniformity of stress distribution due to the stress concentration effect of pores and variations in microstructure. In addition, many of these models neglect the effects of changes in the size and shape of pores as well as the formation of new pores and microcracks during deformation. Previous experimental results also show wide variations in strength at constant porosity [4] indicating that at best these models may only estimate a range of strengths for a

given porosity. Furthermore, many of the relationships have only been modeled over discrete ranges of porosity and therefore may not be applicable for the porosity levels examined here.

4.5 Conclusions

In this study, micropillar compression experiments of ferrite and martensite in dual phase precipitation hardened steel were conducted and the overall bulk behavior was predicted based on the constitutive behavior of the microscopic phases. The following conclusions were drawn:

- Increased yield and tensile strengths of the bulk steel were observed with aging and were attributed to precipitation hardening from the presence of copper and relief of internal stress from carbon diffusion and tempering of the martensite.
- Micropillar compression tests showed higher strengths for martensite than ferrite. The ferrite tests exhibit increased yield stress and nearly constant fracture stress with aging. Martensite, however, showed both increased yield and fracture stress with aging, which is consistent with tensile testing results. Due to this fact and martensite's high phase fraction (92%), martensite is the primary driver to increased strength in the bulk composite steel.
- Due to the high martensite fraction, a conventional rule of mixtures approach was applied to micropillar compression results of the individual microconstituents to calculate the fracture strengths for the composite steels. The effect of porosity was also incorporated and this resulted in

reasonable agreement with the ultimate tensile strengths from tensile tests of the dual phase steels.

4.6 References

1. Introducing Powder Metallurgy (PM), www.mpif.org.
2. R.J. Boucier, D.A. Koss, R.E. Smelser, O. Richmond, Acta Metall. 34 (12) (1986) 2443-2453.
3. G. Straffelini, Powder Metallurgy 48 (2) (2005) 189-192.
4. A. Salak, V. Miskovic, E. Dudrova, E. Rudnayova, Powder Metall Intl, v6 is 3 (1974) 128-132.
5. E. Klar, P. Samal, "Powder Metallurgy Stainless Steels, Processing, Microstructures, and Properties," ASM International, Materials Park, OH (2007).
6. V.T. Troshchenko, translated from Poroshkovaya Metallurgiya, No. 3 (15) (1963) 3-11.
7. R. Haynes, Powder Metall, v14, no27 (1971) 64-70.
8. N.A. Fleck, R.A. Smith, Powder Metall, 24 (3) (1981) 126-130.
9. P.S. Liu, C. Fu, T. Li, Trans Nonferrous Met Soc China, 9 (1) (1999) 70-78.
10. H.E. Exner, D. Pohl, Powder Metall Intl, 10 (4) (1978) 193-196.
11. M. Eudier, Powder Metall, 9 (1962) 278.
12. C.T. Schade, T.F. Murphy, A. Lawley and R. Doherty, Intl J Powder Metall 45 (1) (2009) 38-46.
13. H.J. Klaar, I.A. El-Sesy, A.H.A. Hussein, Steel Research, 61 (2) (1990) 85-92.
14. B. Grushko, B.Z. Weiss, Scripta Metall 23 (1989) 865-870.
15. D.K. Matlock, G. Krauss, L. Ramos, and G.S. Huppi, A Correlation of Processing Variables with Deformation Behavior of Dual-Phase Steels, in *Structure and Properties of Dual-Phase Steels,* American Institute of Mining, Metallurgical, and Petroleum Engineers, 1979, 62-90.

16. M. Erdogan, R. Priestner, Mater Sci and Tech 15 (1999) 1273-1284.

17. M.S. Rashid, Annual Review of Materials Science, 11 (1981) 245-266.

18. G.R. Speich, R.L. Miller, Mechanical Properties of Ferrite-Martensite Steels, in *Structure and Properties of Dual-Phase Steels*, American Institute of Mining, Metallurgical, and Petroleum Engineers, 1979, 145-182.

19. I. Tamura, Y. Tomota, M. Ozawa, Proceedings 3rd Intl Conf on the Strength of Metals and Alloys, Cambridge, Vol. 1, 1973, 611.

20. P.R. Rios, J.R.C. Guimarães, K.K. Chawla, Scripta Metall, 15 (1981) 899-904.

21. M. Delince, P.J. Jacques, T. Pardoen, Acta Materialia 54 (2006) 3395-3404.

22. V.H.B. Hernandez, S.K. Panda, Y. Okita, N.Y. Zhou, J Mater Sci 45 (2010) 1638-1647.

23. V.H.B. Hernandez, S.K. Panda, M.L Kuntz, Y. Zhou, Materials Letters 64 (2010) 207-210.

24. J.L. Stewart, J.J. Williams, N. Chawla, Metall Mater Trans, (2011) submitted.

25. W.D. Nix, H. Gao, J Mech Phys Solids, 46 (1998) 411-425.

26. M.D. Uchic, D.M. Dimiduk, J.N. Florando, W.D. Nix, Science, 305 (2004) 986-989.

27. M.D. Uchic, D.M. Dimiduk, Mat Sci Engr A, 400-401 (2005) 268-278.

28. J.R. Greer, W.C. Oliver, W.D. Nix, Acta Materialia 53 (2005) 1821-1830.

29. J.R. Greer, W.D. Nix, Appl Phys A, 80 (2005) 1625–1629.

30. C. Motz, T. Schöberl, R. Pippan, Acta Mater, 53 (2005) 4269-4279.

31. W.D. Nix, J.R. Greer, G. Feng, E.T. Lilleodden, Thin Solid Films, 515 (2007) 3152-3157.

32. C.P. Frick, B.G. Clark, S. Orso, A.S. Schneider, E. Arzt, Mat Sci Engr A, 489 (2008) 319-329.

33. A.S. Schneider, B.G. Clark, P.A. Gruber, E. Arzt, Mat Sci Engr A, 508 (2009) 241-246.

34. L. Jiang, N. Chawla, Scripta Mater, 63 (2010) 480-483.

35. M.A. Pouchon, J. Chen, R. Ghisleni, J. Michler, W. Hoffelner, Exper Mech, 50 (2010) 79-84.

36. G.F. Vander Voort, G.M. Lucas, E.P. Manilova, Metallography and Microstructures of Stainless Steels and Maraging Steels, ASM Handbook 9 (2004) 670-700.

37. H. Bei, S. Shim, M.K. Miller, G.M. Pharr, E.P. George. Appl Phys Lett, 91 (2007) 111915.

38. W.C. Oliver, G.M. Pharr, J Mater Res 7 (1992) 1564

39. R.E. Reed-Hill, R. Abbaschian, Physical Metallurgy Principles, 3rd ed. Boston, MA: PWS Publishing Company, 1994.

40. S.K. Dhua, A. Ray, D.S. Sarma, Mater Sci Eng A318 (2001) 197-210.

41. S.K. Ghosh, A. Haldar, P.P. Chattopadhyay, J Mater Sci 44 (2009) 580-590.

42. J. Holmes, R.A. Queeney, Powder Metall 28 (1985) 231.

43. K.M. Vedula, R.W. Heckel, Modern Developments in Powder Metallurgy, Metal Powder Industries Federation, Princeton, NJ, 1981.

44. N. Chawla, X. Deng, Mater Sci Eng A 390 (2005) 98-112.

45. A. Hadrboletz, B. Weiss, Intl Mater Rev 42 (1997) 1-44.

46. S.J. Polasik, J.J. Williams, N. Chawla, Metall Mater Trans A 33A (2002) 73.

47. D.R.P. Singh, N. Chawla, G. Tang, Y.-L. Shen, Acta Mater, 58 (2010) 6628-6636.

Chapter 5

CONCLUSIONS

In this study, the microstructure and mechanical behavior of PM dual phase precipitation hardened stainless steels of varying phase fraction and aging temperature were examined. Furthermore, the mechanical behavior of the individual ferrite and martensite microconstituents were characterized by nanoindentation and micropillar fabrication and compression. The following high level conclusions were drawn:

- Higher martensite content resulted in higher yield and ultimate strengths and lower ductility of the bulk steels as expected from the composite microstructure in which martensite imparts strength while ferrite imparts ductility. Specimens with higher martensite content also exhibited lower ductility due to the lower ferrite fraction, increased continuity of the martensite around the ferrite, and higher porosity.
- Regardless of phase fractions, the yield and ultimate tensile strengths of the bulk steels were also observed to increase with increased aging temperature reaching maxima at 538^{o}C. This behavior is attributed to precipitation hardening from the presence of copper and stress relief from carbon diffusion and tempering of the martensite. At higher temperatures, overaging occurs in which precipitates coarsen and the strength decreases. The ductility was also observed to increase slightly with aging due to tempering of the martensite.

- Higher porosity resulted in lower Young's modulus of the bulk steels. The Young's modulus of the fully dense material, which was determined from extrapolation of the experimental data, agreed very well with the theoretical value obtained using the R-A model, suggesting little influence of pore shape and morphology on the elastic properties of the material.
- Nanoindentation of the microconstituents showed higher hardness for martensite than ferrite in all cases, owing to martensite's high dislocation density and tetragonal lattice supersaturated with carbon.
- Both the martensite and ferrite hardness values were shown to increase with increased aging temperature and in many cases showed peak hardness at 538^{o}C which is consistent with bulk tensile test results. Since precipitates in the matrix are exceedingly smaller than the indentation volume currently used, the nanoindentation results include contributions from both the matrix and its precipitates and show that both the ferrite and martensite benefit from precipitation hardening.
- Micropillar compression tests of the HM specimens show higher strengths for martensite than ferrite as expected. The ferrite tests exhibit increased yield stress and nearly constant fracture stress with aging. Martensite, however, shows both increase yield and fracture stresses with aging, which is consistent with tensile testing. Due to this fact and martensite's high phase fraction (92%), results suggest that martensite is the primary driver to increased strength in the bulk composite steel. It should be noted

that these tests exclude contributions from macroscale features such as grain boundaries and microstructural constraint.

- Due to the high martensite fraction, a conventional rule of mixtures approach was applied to micropillar compression results of the individual microconstituents to generate stress-strain curves for the composite steel. Further processing to incorporate the effect of porosity resulted in good agreement with the ultimate tensile strength of the bulk steels.

REFERENCES

1. Introducing PM, Available: www.mpif.org

2. R.J. Boucier, D.A. Koss, R.E. Smelser, O. Richmond, Acta Metall. 34 (12) (1986) 2443-2453.

3. G. Straffelini, Powder Metallurgy 48 (2) (2005) 189-192.

4. J. Holmes, R.A. Queeney, Powder Metall 28 (1985) 231.

5. H.E. Exner, D. Pohl, Powder Metall Intl 10 (1978) 193-196.

6. X. Deng, G.B. Piotrowski, J.J. Williams, N. Chawla, Intl J of Fatigue 27 (2005) 1233-1243.

7. A. Hadrboletz, B. Weiss, Intl Mater Rev 42 (1997) 1-44.

8. S.J. Polasik, J.J. Williams, N. Chawla, Metall Mater Trans A 33A (2002) 73.

9. N. Chawla, X. Deng, Mat Sci Eng A 390 (2005) 98-112.

10. K.M. Vedula, R.W. Heckel, Modern Developments in Powder Metallurgy, Metal Powder Industries Federation, Princeton, NJ, 1981.

11. M. Eudier, Powder Metall, 9 (1962) 278.

12. V.T. Troshchenko, translated from Poroshkovaya Metallurgiya, No. 3 (15) (1963) 3-11.

13. R. Haynes, Powder Metall, v14, no27 (1971) 64-70.

14. A. Salak, V. Miskovic, E. Dudrova, E. Rudnayova, Powder Metall Intl, v6 is 3 (1974) 128-132.

15. N.A. Fleck, R.A. Smith, Powder Metall, 24 (3) (1981) 126-130.

16. P.S. Liu, C. Fu, T. Li, Trans Nonferrous Met Soc China, 9 (1) (1999) 70-78.

17. P.S. Liu, X.S. Wang, H.Y. Luo, Mat Sci and Tech, 19 (2003) 985-986.

18. E. Klar, P. Samal, "Powder Metallurgy Stainless Steels, Processing, Microstructures, and Properties," ASM International, Materials Park, OH (2007).

19. C.T. Schade, T.F. Murphy, A. Lawley and R. Doherty, Intl J Powder Metall 45 (1) (2009) 38-46.

20. H.J. Klaar, I.A. El-Sesy, A.H.A. Hussein, Steel Research, 61 (2) (1990) 85-92.

21. B. Grushko, B.Z. Weiss, Scripta Metall 23 (1989) 865-870.

22. D.K. Matlock, G. Krauss, L. Ramos, and G.S. Huppi, A Correlation of Processing Variables with Deformation Behavior of Dual-Phase Steels, in *Structure and Properties of Dual-Phase Steels*, American Institute of Mining, Metallurgical, and Petroleum Engineers, 1979, 62-90.

23. M. Erdogan, R. Priestner, Mater Sci and Tech 15 (1999) 1273-1284.

24. M.S. Rashid, Annual Review of Materials Science, 11 (1981) 245-266.

25. I. Tamura, Y. Tomota, M. Ozawa, Proceedings 3rd Intl Conf on the Strength of Metals and Alloys, Cambridge, Vol. 1, 1973, 611.

26. G.R. Speich, R.L. Miller, Mechanical Properties of Ferrite-Martensite Steels, in *Structure and Properties of Dual-Phase Steels*, American Institute of Mining, Metallurgical, and Petroleum Engineers, 1979, 145-182.

27. S. Gunduz, B. Demir, R. Kacar. Ironmaking and Steelmaking 35 (1) (2008) 63-68.

28. Z. Jiang, Z. Guan, J. Lian, Mater Sci and Eng A 190 (1995) 55-64.

29. A. Gural, S. Tekeli, T. Ando, J Mater Sci 41 (2006) 7894-7901.

30. M. Sarwar, R. Priestner, J Mater Sci 31 (1996) 2091-2095.

31. A. Bag, K.K. Ray, E.S. Dwarakadasa, Metall Mater Trans A 30A (1999) 1193-1202.

32. P.R. Rios, J.R.C. Guimarães, K.K. Chawla, Scripta Metall, 15 (1981) 899-904.

33. P.H. Chang, A.G. Preban, Acta Metall 35 (5) (1985) 897-903.

34. K. Kocatepe, M. Cerah, M. Erdogan, J Mater Processing Technology 178 (2006) 44-51.

35. S.K. Ghosh, A. Haldar, P.P. Chattopadhyay, J Mater Sci 44 (2009) 580-590.

36. C.N. Hsaio, C.S. Chiou, J.R. Yang, Mater Chem Phys 74 (2002) 134-142.

37. S.K. Dhua, A. Ray, D.S. Sarma, Mater Sci Eng A318 (2001) 197-210.

38. T. Ohmura, K. Sawada, K. Kimura, K. Tsuzaki, Mater Sci Eng A 489 (2008) 85-92.

39. L. Pussegoda and W.R. Tyson, Can. Metall. Q. 23 (1984) 341-347.

40. J. Moon, S. Kim, J. Jang, J. Lee, C. Lee, Mater Sci and Eng A 487 (2008) 552-557.

41. M. Delince, P.J. Jacques, T. Pardoen, Acta Materialia 54 (2006) 3395-3404.

42. T. Ohmura, K. Tsuzaki, S. Matsuoka, Scripta Materialia 45 (2001) 889-894.

43. Y. Choi, W.Y. Choo, D. Kwon, Scripta Materialia 45 (2001) 1401-1406.

44. T.H. Ahn, K.K. Um, J.K. Choi, D.H. Kim, K.H. Oh, M. Kim, H.N. Han, Mater Sci Eng A 523 (2009) 173-177.

45. J. Jang, J Mater Res 22 (1) (2007) 175-185.

46. T. Ohmura, K. Tsuzaki, J Phys D: Appl Phys 41 (2008) 1-6.

47. T.B. Britton, D. Randman, A.J. Wilkinson, J Mater Res 24 (3) (2009) 607-615.

48. T. Ohmura, T. Hara, K. Tsuzaki, Scripta Materialia 49 (2003) 1157-1162.

49. T. Ohmura, K. Tsuzaki, S. Matsuoka, Philosophical Magazine A 82 (10) (2002) 1903-1910.

50. V.H.B. Hernandez, S.K. Panda, Y. Okita, N.Y. Zhou, J Mater Sci 45 (2010) 1638-1647.

51. V.H.B. Hernandez, S.K. Panda, M.L Kuntz, Y. Zhou, Materials Letters 64 (2010) 207-210.

52. W.D. Nix, H. Gao, J Mech Phys Solids, 46 (1998) 411-425.

53. J.R. Greer, W.C. Oliver, W.D. Nix, Acta Materialia 53 (2005) 1821-1830.

54. J.R. Greer, W.D. Nix, Appl Phys A, 80 (2005) 1625–1629.

55. W.D. Nix, J.R. Greer, G. Feng, E.T. Lilleodden, Thin Solid Films, 515 (2007) 3152-3157.

56. M.D. Uchic, D.M. Dimiduk, J.N. Florando, W.D. Nix, Science, 305 (2004) 986-989.

57. M.D. Uchic, D.M. Dimiduk, Mat Sci Engr A, 400-401 (2005) 268-278.

58. C.P. Frick, B.G. Clark, S. Orso, A.S. Schneider, E. Arzt, Mat Sci Engr A, 489 (2008) 319-329.

59. C. Motz, T. Schöberl, R. Pippan, Acta Mater, 53 (2005) 4269-4279.

60. H. Tang, K.W. Schwarz, H.D. Espinosa, Acta Mater, 55 (2007) 1607-1616.

61. A.S. Schneider, B.G. Clark, P.A. Gruber, E. Arzt, Mat Sci Engr A, 508 (2009) 241-246.

62. M.A. Pouchon, J. Chen, R. Ghisleni, J. Michler, W. Hoffelner, Exper Mech, 50 (2010) 79-84.

Chapter 3

1. Introducing PM, Available: www.mpif.org

2. R.J. Boucier, D.A. Koss, R.E. Smelser, O. Richmond, Acta Metall. 34 (12) (1986) 2443-2453.

3. G. Straffelini, Powder Metallurgy 48 (2) (2005) 189-192.

4. J. Holmes, R.A. Queeney, Powder Metall 28 (1985) 231.

5. H.E. Exner, D. Pohl, Powder Metall Intl 10 (1978) 193-196.

6. X. Deng, G.B. Piotrowski, J.J. Williams, N. Chawla, Intl J of Fatigue 27 (2005) 1233-1243.

7. A. Hadrboletz, B. Weiss, Intl Mater Rev 42 (1997) 1-44.

8. S.J. Polasik, J.J. Williams, N. Chawla, Metall Mater Trans A 33A (2002) 73.

9. C.T. Schade, T.F. Murphy, A. Lawley and R. Doherty, Intl J Powder Metall 45 (1) (2009) 38-46.

10. H.J. Klaar, I.A. El-Sesy, A.H.A. Hussein, Steel Research, 61 (2) (1990) 85-92.

11. B. Grushko, B.Z. Weiss, Scripta Metall 23 (1989) 865-870.

12. D.K. Matlock, G. Krauss, L. Ramos, and G.S. Huppi, A Correlation of Processing Variables with Deformation Behavior of Dual-Phase Steels, in *Structure and Properties of Dual-Phase Steels,* American Institute of Mining, Metallurgical, and Petroleum Engineers, 1979, 62-90.

13. M. Erdogan, R. Priestner, Mater Sci and Tech 15 (1999) 1273-1284.

14. M.S. Rashid, Annual Review of Materials Science, 11 (1981) 245-266.

15. I. Tamura, Y. Tomata, A. Okao, Y. Yamaoha, H. Ozawa, S. Kaotoni, Trans Iron Steel Inst Jpn 13 (1973) 283-292.

16. G.R. Speich, R.L. Miller, Mechanical Properties of Ferrite-Martensite Steels, in *Structure and Properties of Dual-Phase Steels*, American Institute of Mining, Metallurgical, and Petroleum Engineers, 1979, 145-182.

17. S. Gunduz, B. Demir, R. Kacar. Ironmaking and Steelmaking 35 (1) (2008) 63-68.

18. Z. Jiang, Z. Guan, J. Lian, Mater Sci and Eng A 190 (1995) 55-64.

19. A. Gural, S. Tekeli, T. Ando, J Mater Sci 41 (2006) 7894-7901.

20. M. Sarwar, R. Priestner, J Mater Sci 31 (1996) 2091-2095.

21. A. Bag, K.K. Ray, E.S. Dwarakadasa, Metall Mater Trans A 30A (1999) 1193-1202.

22. P.H. Chang, A.G. Preban, Acta Metall 35 (5) (1985) 897-903.

23. K. Kocatepe, M. Cerah, M. Erdogan, J Mater Processing Technology 178 (2006) 44-51.

24. S.K. Ghosh, A. Haldar, P.P. Chattopadhyay, J Mater Sci 44 (2009) 580-590.

25. C.N. Hsaio, C.S. Chiou, J.R. Yang, Mater Chem Phys 74 (2002) 134-142.

26. S.K. Dhua, A. Ray, D.S. Sarma, Mater Sci Eng A318 (2001) 197-210.

27. T. Ohmura, K. Sawada, K. Kimura, K. Tsuzaki, Mater Sci Eng A 489 (2008) 85-92.

28. L. Pussegoda and W.R. Tyson, Can. Metall. Q. 23 (1984) 341-347.

29. J. Moon, S. Kim, J. Jang, J. Lee, C. Lee, Mater Sci and Eng A 487 (2008) 552-557.

30. M. Delince, P.J. Jacques, T. Pardoen, Acta Materialia 54 (2006) 3395-3404.

31. T. Ohmura, K. Tsuzaki, S. Matsuoka, Scripta Materialia 45 (2001) 889-894.

32. Y. Choi, W.Y. Choo, D. Kwon, Scripta Materialia 45 (2001) 1401-1406.

33. T.H. Ahn, K.K. Um, J.K. Choi, D.H. Kim, K.H. Oh, M. Kim, H.N. Han, Mater Sci Eng A 523 (2009) 173-177.

34. J. Jang, J Mater Res 22 (1) (2007) 175-185.

35. T. Ohmura, K. Tsuzaki, J Phys D: Appl Phys 41 (2008) 1-6.

36. T.B. Britton, D. Randman, A.J. Wilkinson, J Mater Res 24 (3) (2009) 607-615.

37. T. Ohmura, T. Hara, K. Tsuzaki, Scripta Materialia 49 (2003) 1157-1162.

38. T. Ohmura, K. Tsuzaki, S. Matsuoka, Philosophical Magazine A 82 (10) (2002) 1903-1910.

39. V.H.B. Hernandez, S.K. Panda, Y. Okita, N.Y. Zhou, J Mater Sci 45 (2010) 1638-1647.

40. V.H.B. Hernandez, S.K. Panda, M.L Kuntz, Y. Zhou, Materials Letters 64 (2010) 207-210.

41. G.F. Vander Voort, G.M. Lucas, E.P. Manilova, Metallography and Microstructures of Stainless Steels and Maraging Steels, ASM Handbook 9 (2004) 670-700.

42. W.C. Oliver, G.M. Pharr, J Mater Res 7 (1992) 1564.

43. N. Chawla, X. Deng, Mat Sci Eng A 390 (2005) 98-112.

44. K.M. Vedula, R.W. Heckel, Modern Developments in Powder Metallurgy, Metal Powder Industries Federation, Princeton, NJ, 1981.

45. R.E. Reed-Hill, R. Abbaschian, Physical Metallurgy Principles, 3rd ed. Boston, MA: PWS Publishing Company, 1994.

46. T. Marcu, A. Molinari, G. Straffelini, and S. Berg, International Journal of Powder Metallurgy 40 (3) (2004) 57-64.

47. W.A. Spitzig, R.E. Smelser, O. Richmond, Acta Metall. 36 (5) (1988) 1201-1211.

48. A. Salak, Ferrous Powder Metallurgy, Cambridge International Science Publishing, Cambridge, 1997.

49. N. Chawla, F. Ochoa, V.V. Ganesh, X. Deng, J Mater Sci: Materials in Electronics 15 (2004) 385-388.

50. N. Ramakrishnan, V.S. Arunachalam, J Am Ceram Soc 76 (1993) 2745.

51. Q. Furnemont, M. Kempf, P.J. Jacques, M. Goken, F. Delannay, Materials Science and Engineering A328 (2002) 26-32.

52. T. Ohmura, K. Tsuzaki, S. Matsuoka, Philosophical Magazine A 82 (10) (2002) 1903-1910.

53. P. Abramowitz, R.A. Moll, Metall Trans 1 (1970) 1773-1775.

54. M. Mazinani, W.J. Poole, Metallurgical and Materials Transactions A 38A (2007) 328-339.

55. K.K. Chawla, P.R. Rios, J.R.C. Guimaraes, Journal of Materials Science Letters 2 (1983) 94-98.

56. H.P. Shen, T.C. Lei, J.Z. Liu, Materials Science and Technology 3 (1987) 415-21.

57. F.M. Al-Abbasi, J.A. Nemes, International Journal of Mechanical Sciences 45 (2003) 1449-1465.

58. E. Maire, O. Bouaziz, M. Di Michiel, C. Verdu, Acta Materialia 56 (2008) 4954-4964.

59. X. Sun, K.S. Choi, W.N. Liu, M.A. Khaleel, International Journal of Plasticity 25 (2009) 1888-1909.

60. R.K. Ray, Scripta Metallurgica 18 (1984) 1205-1209.

Chapter 4:

1. Introducing Powder Metallurgy (PM), www.mpif.org.

2. R.J. Boucier, D.A. Koss, R.E. Smelser, O. Richmond, Acta Metall. 34 (12) (1986) 2443-2453.

3. G. Straffelini, Powder Metallurgy 48 (2) (2005) 189-192.

4. A. Salak, V. Miskovic, E. Dudrova, E. Rudnayova, Powder Metall Intl, v6 is 3 (1974) 128-132.

5. E. Klar, P. Samal, "Powder Metallurgy Stainless Steels, Processing, Microstructures, and Properties," ASM International, Materials Park, OH (2007).

6. V.T. Troshchenko, translated from Poroshkovaya Metallurgiya, No. 3 (15) (1963) 3-11.

7. R. Haynes, Powder Metall, v14, no27 (1971) 64-70.

8. N.A. Fleck, R.A. Smith, Powder Metall, 24 (3) (1981) 126-130.

9. P.S. Liu, C. Fu, T. Li, Trans Nonferrous Met Soc China, 9 (1) (1999) 70-78.

10. H.E. Exner, D. Pohl, Powder Metall Intl, 10 (4) (1978) 193-196.

11. M. Eudier, Powder Metall, 9 (1962) 278.

12. C.T. Schade, T.F. Murphy, A. Lawley and R. Doherty, Intl J Powder Metall 45 (1) (2009) 38-46.

13. H.J. Klaar, I.A. El-Sesy, A.H.A. Hussein, Steel Research, 61 (2) (1990) 85-92.

14. B. Grushko, B.Z. Weiss, Scripta Metall 23 (1989) 865-870.

15. D.K. Matlock, G. Krauss, L. Ramos, and G.S. Huppi, A Correlation of Processing Variables with Deformation Behavior of Dual-Phase Steels, in *Structure and Properties of Dual-Phase Steels,* American Institute of Mining, Metallurgical, and Petroleum Engineers, 1979, 62-90.

16. M. Erdogan, R. Priestner, Mater Sci and Tech 15 (1999) 1273-1284.

17. M.S. Rashid, Annual Review of Materials Science, 11 (1981) 245-266.

18. G.R. Speich, R.L. Miller, Mechanical Properties of Ferrite-Martensite Steels, in *Structure and Properties of Dual-Phase Steels*, American Institute of Mining, Metallurgical, and Petroleum Engineers, 1979, 145-182.

19. I. Tamura, Y. Tomota, M. Ozawa, Proceedings 3rd Intl Conf on the Strength of Metals and Alloys, Cambridge, Vol. 1, 1973, 611.

20. P.R. Rios, J.R.C. Guimarães, K.K. Chawla, Scripta Metall, 15 (1981) 899-904.

21. M. Delince, P.J. Jacques, T. Pardoen, Acta Materialia 54 (2006) 3395-3404.

22. V.H.B. Hernandez, S.K. Panda, Y. Okita, N.Y. Zhou, J Mater Sci 45 (2010) 1638-1647.

23. V.H.B. Hernandez, S.K. Panda, M.L Kuntz, Y. Zhou, Materials Letters 64 (2010) 207-210.

24. J.L. Stewart, J.J. Williams, N. Chawla, Metall Mater Trans, (2011) submitted.

25. W.D. Nix, H. Gao, J Mech Phys Solids, 46 (1998) 411-425.

26. M.D. Uchic, D.M. Dimiduk, J.N. Florando, W.D. Nix, Science, 305 (2004) 986-989.

27. M.D. Uchic, D.M. Dimiduk, Mat Sci Engr A, 400-401 (2005) 268-278.

28. J.R. Greer, W.C. Oliver, W.D. Nix, Acta Materialia 53 (2005) 1821-1830.

29. J.R. Greer, W.D. Nix, Appl Phys A, 80 (2005) 1625–1629.

30. C. Motz, T. Schöberl, R. Pippan, Acta Mater, 53 (2005) 4269-4279.

31. W.D. Nix, J.R. Greer, G. Feng, E.T. Lilleodden, Thin Solid Films, 515 (2007) 3152-3157.

32. C.P. Frick, B.G. Clark, S. Orso, A.S. Schneider, E. Arzt, Mat Sci Engr A, 489 (2008) 319-329.

33. A.S. Schneider, B.G. Clark, P.A. Gruber, E. Arzt, Mat Sci Engr A, 508 (2009) 241-246.

34. L. Jiang, N. Chawla, Scripta Mater, 63 (2010) 480-483.

35. M.A. Pouchon, J. Chen, R. Ghisleni, J. Michler, W. Hoffelner, Exper Mech, 50 (2010) 79-84.

36. G.F. Vander Voort, G.M. Lucas, E.P. Manilova, Metallography and Microstructures of Stainless Steels and Maraging Steels, ASM Handbook 9 (2004) 670-700.

37. H. Bei, S. Shim, M.K. Miller, G.M. Pharr, E.P. George. Appl Phys Lett, 91 (2007) 111915.

38. W.C. Oliver, G.M. Pharr, J Mater Res 7 (1992) 1564

39. R.E. Reed-Hill, R. Abbaschian, Physical Metallurgy Principles, 3rd ed. Boston, MA: PWS Publishing Company, 1994.

40. S.K. Dhua, A. Ray, D.S. Sarma, Mater Sci Eng A318 (2001) 197-210.

41. S.K. Ghosh, A. Haldar, P.P. Chattopadhyay, J Mater Sci 44 (2009) 580-590.

42. J. Holmes, R.A. Queeney, Powder Metall 28 (1985) 231.

43. K.M. Vedula, R.W. Heckel, Modern Developments in Powder Metallurgy, Metal Powder Industries Federation, Princeton, NJ, 1981.

44. N. Chawla, X. Deng, Mater Sci Eng A 390 (2005) 98-112.

45. A. Hadrboletz, B. Weiss, Intl Mater Rev 42 (1997) 1-44.

46. S.J. Polasik, J.J. Williams, N. Chawla, Metall Mater Trans A 33A (2002) 73.

47. D.R.P. Singh, N. Chawla, G. Tang, Y.-L. Shen, Acta Mater, 58 (2010) 6628-6636.